PROPAGATION AND SOURCE PARAMETERS FROM LONG-PERIOD HIGH-GAIN SEISMOGRAPHS

Agustin Udias

Barcelona University

Prepared for:

Air Force Office of Scientific Research
Advanced Research Projects Agency

May 1975

PROPAGATION AND SOURCE PARAMETERS FROM LONG-PERIOD HIGH-GAIN SEISMOGRAPHS

FINAL REPORT

DEPARTAMENTO DE FISICA DE LATIERRA Y DEL COSMOS

UNIVERSIDAD DE BARCELONA

SPAIN

PREPARED UNDER GRANT AFOSR 74-2609

WITH THE AIR FORCE OFFICE OF SCIENTIFIC RESEARCH

SPONSORED BY

ADVANCED RESEARCH PROJECT AGENCY

ARPA ORDER No. 1827

MAY 1975

SECURITY CLASSIFICATION OF THIS PAGE (When Data Entered)

REPORT DOCUMENTATION PAGE

READ INSTRUCTIONS BEFORE COMPLETING FORM

1. REPORT NUMBER: AFOSR - TR - 75 - 1071	2. GOVT ACCESSION NO.
3. RECIPIENT'S CATALOG NUMBER	
4. TITLE (and Subtitle): Propagation and Source Parameters from Long-Period High-Gain Seismographs	5. TYPE OF REPORT & PERIOD COVERED: Final Technical, 1 Oct 1973 -31 Mar 1975
	6. PERFORMING ORG. REPORT NUMBER
7. AUTHOR(s): Agustin Udias	8. CONTRACT OR GRANT NUMBER(s): AFOSR-74-2609
9. PERFORMING ORGANIZATION NAME AND ADDRESS: Department of Terrestrial and Cosmic Physics, University of Barcelona, Ada. Gmo. Franco, 647 Barcelona - 14 Spain	10. PROGRAM ELEMENT, PROJECT, TASK AREA & WORK UNIT NUMBERS: 62701E, AO 1827
11. CONTROLLING OFFICE NAME AND ADDRESS: ARPA/NMR, 1400 Wilson Blvd., Arlington, VA 22209	12. REPORT DATE: May 1975
	13. NUMBER OF PAGES: 80
14. MONITORING AGENCY NAME & ADDRESS (if different from Controlling Office): AFOSR/NP, 1400 Wilson Blvd., Arlington, VA 22209	15. SECURITY CLASS. (of this report): Unclassified
	15a. DECLASSIFICATION/DOWNGRADING SCHEDULE

16. DISTRIBUTION STATEMENT (of this Report)

Approved for public release; distribution unlimited

17. DISTRIBUTION STATEMENT (of the abstract entered in Block 20, if different from Report)

18. SUPPLEMENTARY NOTES

19. KEY WORDS (Continue on reverse side if necessary and identify by block number)

Seismology
Attenuation
Earthquake Parameters
Phase Velocity
Seismic Wave Propagation

20. ABSTRACT (Continue on reverse side if necessary and identify by block number)

Seismic moment, length and stress condition at the source of four earthquakes of magnitude about 5, attenuation coeficients of Rayleigh waves for nuclear explosions and phase velocities across the Mediterranean Sea are determined and analysed. In all cases results from HGLP stations are compared with those from WWSSN stations.

DD FORM 1 JAN 73 1473 EDITION OF 1 NOV 65 IS OBSOLETE

SECURITY CLASSIFICATION OF THIS PAGE (When Data Entered)

Form approved
Budget Bureau No.22-R0293

Departamento de Física de la Tierra y del Cosmos
Universidad de Barcelona
Barcelona, Spain

Final Report
May, 1975

ARPA order No. 1827
Program Code No. 4F10
Contractor - Departamento de Física de la Tierra y del Cosmos
Universidad de Barcelona
Effective Date of Contract 1 Oct, 1973
Contractor Expiration Date 31 Mar, 1975
Amount of Contract - $ 19,813
Grant Number, AFOSR -74- 2609
Report Period: 1 Oct 73 - 30 Sep 74
Principal Investigator - Agustin Udias
3214300
Title of Work: Propagation and Source Parameters from
Long-Period High-Gain Seismographs.

Sponsored by
Advanced Research Project Agency
ARPA order No. 1827

PROPAGATION AND SOURCE PARAMETERS FROM LONG-PERIOD HIGH-GAIN SEISMOGRAPHS

DETERMINATION OF SOURCE PARAMETERS FROM THE SPECTRA OF SURFACE AND BODY WAVES USING HIGH-GAIN LONG-PERIOD STATIONS.

Agustín Udías and Antonio Correig
Universided de Barcelone

ABSTRACT

Records from high-gain long-period stations have been used in the determination of source paremeters of four shellow eerthquekes of magnitude between 5 end 6 from the anelysis of the spectra of Reyleigh end shear waves. Results show a good agreement between the paremeters derived from both types of waves. Seismic moments are of the order of 10^{24} dyne-cm, stress drops consistently low between 0.1 and 1 bar and epparent average stresses between 1 end 30 bars.

INTRODUCTION

Since 1970 eleven stations with high-gein (magnifications up to 150,000) end long period (peak between 30 end 50 seconds) systems recording in analog and digital form have been put into operation (Sevino et al., 1972). These stetions, that will be referred to as HGLP, have been used in the determinetion of source mechanism parameters, comparing their performance with that of the World Wide Stendard Station Net (WWSSN) stations. Locations of the HGLP stetions whose data have been used in this study ere given in table 1.

A very important step in the analysis of the HGLP data is the preliminary processing which involves enalog to digital conversion, filtering, spectral analysis end reduc-

tion to ground motion. The HGLP instruments have two outputs, one enelog (HGLP-ANL) with conventionel photogrephic recording the other digitel (HGPL-DIG) on magnetic tape. Digitalization of the analog records have been done from enlarged copies of the microfilms. In this respect the data from earthquekes reletively large end near to the station ere practically impossible to analyze. Amplitudes ere too large, lines feinted, and traces entengled. The digitel outputs should solve this problem, but it creates some of its own.

In order to study the capebilities of the digitel outputs of the HGLP stetions, the digital tapes in file at the Lemont-Doherty Observetory were studied. Some of the problems found were the following; records not in the Lamont fils, copies defective, feilures present in the digital system, and too low magnificetions. The process of finding the proper place in the tepes is also very time consuming, since there is not a fast seerch system. Another problem encountered in using HGLP-DIG deta is the variation of the conversion fector to ground motion. In the ALQ (Albuquerque Observetory) stetion the values found in 10 calibretions from Oct 73 to Mar 74 give for the magnification et 30 sec in counts per micron values ranging from 802 to 1232 in the Z component, 512 to 852 in NS and 593 to 965 in EW (A. Murphy, personel comunication). It is not known whether the chenges were the result of modifications made to the system or sponteneous chenges. If the letter is true, large errors can be introduced when using digitel deta from stations where calibretion is not repeated so often. This lack of stability in the digital system would be reflected in the comparison of the source perameters which require ground motion

reduction as determined from analog and digital records.

SOURCE PARAMETERS AND THE SPECTRUM OF SEISMIC WAVES

For many yeers all that could be found about the mechanism of earthquakes was the orientation of the two nodal planes of P waves, one of them corresponding to the plane of fracture and the energy released as seismic waves derived usually from magnitude. Progress in the study of focal mechanism in the last ten years has led to the definition and determination of several parameters describing more fully the processes at the source of earthquakes, such as the fracture dimensions, dislocation, seismic moment, average stress and stress drop. Dislocation dynamic models of the source of earthquakes predict the shape of the spectrum of seismic waves for the far displacement field. From the parameters which define the form of such spectrum certain important characteristics of the dimensions and stress conditions at the source can be determined. Many authors have in the recent years treated this problem, among them, Aki (1967, 1972) Ben Menahen (1961, 1965), Brune (1970), Hanks and Thatcher (1972), Hanks and Wyss (1972), Dahlen (1974).

In general lines the spectrum of seismic waves at the far field can be described as consisting of a low frequency flat part of amplitude Ω_o followed by a decay of amplitude with frequency starting at a particular frequency f_o called the "corner frequency". The way spectral amplitude decay with frequency is governed by the parameter ε . For a particular case when $\varepsilon = 1$, the spectral amplitudes decay approximately as the inverse of the square of frequency. This case represents a dislocation in which the stress drop is complete. These three parameters of the spectrum can be

TABLE 1

High-Gain Long-Period station locations.

Station Code	Station Name	Location	Elevation Meters
OGD	Ogdensburg New Jersey	41°04'00N ; 74°37'00W	-373
CHG	Chiang Mai Thailand	18°47'24''N; 98°58'37''W	416
EIL	Eilat Israel	29°33'00''N; 34°57'00''E	
FBK	Fairbanks Alaska	64°53'58''N;148°00'20''W	330
TLO	Toledo Spain	39°51'36''N; 4°00'53''W	465
KON	Kongsberg Norway	59°38'57''N; 9°37'55''E	200
ALQ	Albuquerque New Mexico	34°56'30''N;106°27'30''W	1853

related to source characteristics. The spectral amplitude level al low frequencies Ω_o is releted to the seismic moment, which for a fracture is defined as the product of the rigidity, area and averege dislocation. The corner frequency f_o is releted to the dimensions of the feult, and ε with the retio of the stress drop to the effective stress. In principle spectre from either body or surface weves can be used in the determination of source parameters. However, surface weves are preferred in the determinetion of seismic moments of large shallow shocks since for these cases the long period spectrel dete of body waves are mixed with later errivels. For smaller and deeper events body waves are found more useful. For the determination of source dimensions from the corner frequency is preferable to use body waves since f_o is generally et a frequency where surface waves depend greatly on propagation conditions (Hanks and Wyss 1972). For the magnitude range ($5 < m < 6$) of the shocks of this study, and shallow depths, surface and body waves can be equally used for the determination of seismic moments. Source dimensions cen be calculated from the corner frequency of shear waves and also from surface waves, but not from the corner frequency, but from the directivity function. In this way for the same shock source perameters can be determined independently from body and surface waves.

Source parameters from spectra of Rayleigh waves

Following the work of Ben-Menehen, Rosenman and Harkrider (1970) the seismic moment $M_o(R)$ cen be expressed in terms of the spectral amplitude et the low frequencies of the vertical component of the Reyleigh wave $\Omega_o(R)$ in the form;

$$M_o(R) = \frac{\mu \Omega_o(R)}{\frac{\exp(-\gamma_R \Delta - i\frac{\pi}{4})}{\sqrt{\sin\frac{\Delta}{a}}}\left(P_R P_R + s_R S_R + i q_R Q_R\right)} \qquad (1)$$

where μ is the rigidity modulus, γ_R the attenuation coefficient of Rayleigh waves, Δ the distance, a the earth radius, and P_R, p_R, S_R, s_R, Q_R, q_R, are the transfer functions for a stratafied earth corresponding to a double couple source. The values of the parameters of this equation are given in convenient table form by Ben-Menahen, Rosenman and Harkrider (1970).

The fault length can be obtained assuming a propagating fracture of rectangular form, from the "directivity function". This function has been defined by Ben-Menahen (1961) as the ratio of the spectral amplitudes of surface waves corresponding to rays leaving the source in opposite directions. The limitation of using only data from stations 180 degrees apart in azimuth is not necessary for faults with large strike slip component (Udías, 1971). If α is the angle between the azimuths of two stations, the length of the fault b is given by

$$b = \frac{c_R}{f_{max}\left(\frac{c_R}{v} - \cos(\theta + \alpha)\right)} = \frac{c_R}{f_{min}\left(\frac{c_R}{v} - \cos\theta\right)} \qquad (2)$$

where f_{max} and f_{min} are the frequencies of the first maximum or minimum of the directivity function, v the rupture velocity, c_R the Rayleigh wave phase velocity and θ the

azimuth from the fault plane to one of the stations.

In order to compare the results of source parameters determined from the spectrum of Rayleigh waves with magnitude, is convenient to calculate it also from surface waves. The following formula has been used here

$$M_S = \log\left(\frac{A}{T}\right) + 1.66 \log \Delta + 3.3 \qquad (3)$$

where A is the amplitude in microns of surface waves corresponding to 20 s period, T the period and the epicentral distance in degrees. From this value of magnitude, the energy can be calculated using the relation (Richter, 1958)

$$\log E_S = 11.8 + 1.5\, M_S \qquad (4)$$

Source parameters from the spectra of S waves

Accepting the general validity of Brune's model (Brune, 1970 and 1971) and the physical interpretation given by him to the three parameters Ω_o, f_o and ε, derived from the spectra of shear waves, they can be used to determine the seismic moment M_o and the dimension r of the equivalent circular dislocation. Here ε is taken to be unity, assuming that the stress drop is complete.

The seismic moment $M_o(s)$ can be determined from the spectral amplitude level at low frequencies $\Omega_o(s)$ of the shear waves using the relation (Hanks and Wyss, 1972)

$$M_o(s) = 4\pi \rho \beta^3 R \Omega_o(s) k e^{\gamma R} \qquad (5)$$

Where β is the shear wave velocity near the source, and R the hypocentral distances. The attenuation coefficient γ is given by

$$\gamma = \frac{\pi}{T Q_\beta \beta}$$

where T is the period and Q_β the average quality factor for shear waves. The factor k corrects for the effect of the radiation pattern and the reflection at the free surface and is given by

$$k = \frac{1}{\sqrt{2}\,\chi(\theta,\varphi)}$$

where $\chi(\theta,\varphi)$ is the normalized radiation pattern for the S - waves from a double couple source.

The corner frequency of the shear waves spectrum $f_o(S)$ is related to the radius of the equivalent circular dislocation r by

$$r = \frac{2.34}{2\pi f_o(S)} \qquad (6)$$

For a comparison between the dimensions defined by r and b, one may consider that 2r represents the width of the rectangular fault and this as 1/3 of the length b. Another relation can be derived from equal area considerations

$$A = \pi r^2 = \frac{1}{3} b^2 \qquad (7)$$

which results in

$$r = \sqrt{\frac{1}{3\pi}}\, b = 0.325\, b \qquad (8)$$

The energy radiated as seismic waves E_s is given as a fraction of the total energy E by

$$E_s = \eta E \qquad (9)$$

where η is the seismic efficiency factor. This energy E_s can be calculated from the body wave magnitude m_b by the standard relation (Richter, 1958)

$$\log E_s = 5.8 + 2.4\, m_b \qquad (10)$$

In terms of $\Omega_o(S)$ and $f_o(S)$ the energy is also given approximately by (Wyss and Hanks, 1972)

$$E_S \cong 8.53\,\pi^3 \rho\,\beta\,R^2\,\Omega_o^2(S) f_o(S)\,k^2 \qquad (11)$$

Average dislocation, average stress and stress drop

From the analysis of either surface or body waves we can independently determine the seismic moment, fault dimensions (radius or length) and seismic energy. From these parameters others can be derived that are useful in order to describe the nature of a seismic source.

For the source of an earthquake considered as a sudden dislocation on a plane surface, the seismic moment is defined as the product of the area of the fault A by the rigidity μ and the average dislocation or displacement over the fault surface $\bar{w}$ (Wyss and Brune, 1968)

$$M_o = \mu A \bar{w} \qquad (12)$$

From this relation the average dislocation is given by

$$\bar{w} = \frac{M_o}{\mu A} \qquad (13)$$

and for the rectangular fault model and the circular one used in the surface and body wave analysis one can write

$$\bar{w}(R) = \frac{3\,M_o(R)}{\mu\,\beta^2} \qquad (14)$$

$$\bar{w}(S) = \frac{M_o(S)}{\mu \pi r^2} \qquad (15)$$

The difference in shear stress acting on a fault surface before and after the occurrence of an earthquake is generally

referred to as the "stress drop" $\Delta\sigma = \sigma_1 - \sigma_2$ This is related to the maximum dislocation w_m through the equation (Brune and Allen, 1967)

$$\Delta\sigma = \xi \frac{w_m \mu}{d} \tag{16}$$

where d is the width of the fault and ξ a constant ranging from 1/2 to $2\pi/3$, depending on fault geometry. For earthquakes with large strike-slip component of motion ξ can be taken as 1/2. The maximum dislocation on a fault is usually taken as 4/3 the average value $\bar{w}$. Taking these relations and the expression for $\bar{w}$ from equation (13) we obtain for the stress drop in a vertical rectangular strike-slip fault with width equal to 1/3 its length

$$\Delta\sigma(R) = \frac{6 M_o(R)}{b^3} \tag{17}$$

This relation is similar to the one given by Brune (1971) for a circular dislocation

$$\Delta\sigma(S) = \frac{7 M_o(S)}{16 r^3} \tag{18}$$

As the stress drop $\Delta\sigma(R)$ depends on the square of the fault width, it is greatly influenced by the assumed relation between fault length and width.

The total energy E released by slipping on a fault can be written as the product of the average shear stress $\bar{\sigma} = \frac{1}{2}(\sigma_1 + \sigma_2)$ acting on the fault plane by the area and the average dislocation

$$E = \bar{\sigma} A \bar{w} \tag{19}$$

From this relation the "apparent average stress" $\eta\bar{\sigma}$, or product of the average stress times the seismic efficiency factor can be obtained as,

$$\eta\bar{\sigma} = \frac{\mu E_s}{M_o} \qquad (20)$$

Since E_s and M_o can be independently calculated from body and surface waves, we can also calculate two values of the apparent stress. The interpretation of the ratio of the seismic energy to the moment depends on the source model. Randall (1972) interprets it as being related to the stress drop instead of the average stress.

SOURCE PARAMETERS OF FOUR EARTHQUAKES

Four earthquakes have been selected in the same magnitude range, $5 < m < 6$; dates, epicenters and origin times are given in table 2 . Three are located in the mid-Atlantic ridge and one in the Aleutian islands. Focal mechanism using first motions of P wave have been determined; solutions are shown in figures 1, 2, 3, and 4, and orientation (strike and dip) of the two planes given in table 2. Solution for shock AZOR represents normal faulting along planes oriented approximately north-south. This solution is consistent with the type of faults present in an expanding ridge. The solution for ALEU is not well defined. The data allows two possible solutions one involving strike-slip motion on vertical planes striking north-south and east-west and the other reverse faulting. For the first type of mechanism the north-south plane which has been taken as the fault plane is consistent with an "arc-arc" transform fault. This type of

TABLE 2

Epicentral and focal mechanism data.

Code	Date	Lat.	Long.	Origin Time	Depth (km)	m_b	FAULT PLANES A	FAULT PLANES B
AZOR	18-NOV-1970	35.1N	35.7W	12h:23:18.0	N	5.6	N39W,60NE	N33E,60NW
ALEU	3-JAN-1972	51.1N	178.E	17h:06:22.3	46	5.5	a)N8E,90	N7W,90
							b)N15E,62	N38W,41E
NAT1	13-MAY-1972	45.0N	28.2W	16h:40:22.0	N	5.0	N15E,51W	N82W,80SW
NAT2	6-JUN-1972	32.9N	39.9W	05h:25:50.2	N	5.5	N58W,88NW	N19E,78NE

faulting is common in the Aleutian Islands (Stauder, 1968). The second solution has no easy tectonic interpretation. Reverse faulting in the Aleutian region give planes with an east-west orientation and underthrusting of the Pacific block under the islands consistent with the subduction movement of the oceanic plate. The solution for NAT1 and NAT2 represent right-lateral strike-slip movement on an east-west fault, motion wich is consistent with transform faults of the mid-Atlantic ridge. In conclusion except for AZOR the mechanism have large strike-slip component of motion.

In figure 1, 2, 3 and 4 the position of the stations used in the Rayleigh wave analysis are shown on the rim of the projection and that of the stations used in the body wave analysis with a large open circle.

Determination of seismic moment and dimensions

Spectra of Rayleigh waves

Spectra of Rayleigh waves have been calculated for a total of 21 stations, of these 6 HGLP and 15 WWSSN. Examples of the spectra are given in figures 5, 6, and 7. All spectra show a well defined constant level of spectral amplitude Ω_o for low frequencies. Figure 9 shows the spectra of the Rayleigh waves in ALQ from the records of the WWSSN and HGPL (analog and digital). The two analog records give very similar spectra.

Determinations of the seismic moment M_o has been done using equation (1) and results are given in table 3. Values are relatively stable and show a good agreement between the determinations based on data from WWSSN stations and HGLP stations. The spectral amplitudes have been mea

TABLE 3

Spectral amplitudes of Rayleigh waves and seismic moments.

STATION	(km)	T = 100 S $M_o(10^{24}$ dyne-cm)		T = 50 S $M_o(10^{24}$ dyne-cm)	
AZOR					
AAE-WWSSN	8025	0.6	1.4	0.6	2.9
BUL	9025	1.8	6.4	2.4	38.0
COP	4290	2.4	3.4	2.6	3.0
LON	7006	1.3	2.1	1.5	5.3
NUR	5079	3.1	4.4	4.4	6.1
ALEU					
ALQ-WWSSN	6057	3.0	2.9	1.4	0.6
MAT	3602	0.8	0.8	0.3	0.1
NOR	5213	0.2	0.2	0.03	0.01
NAT1					
EIL-HGLP(AN)	5706	0.4	0.6	0.16	0.2
KON	2293	1.0	1.6	0.19	0.2
OGD	3758	2.3	3.1	0.45	0.3
GDH-WWSSN	3054	6.0	8.3	2.3	1.3
KON	2993	2.0	3.3	1.8	1.5
VAL	1530	5.5	8.0	3.3	1.4
NAT2					
ALQ-HGLP(AN)	6041	2.9	9.0	1.4	1.6
-HGLP(DTS)		1.1	3.4	0.2	0.2
-WWSSN		9.2	29.0	3.2	3.6
KON-HGLP(AN)	4671	1.3	1.9	0.06	0.03
TLO	3285	2.9	4.4	0.6	0.6
LPB-WWSSN	6263	0.3	0.8	0.05	0.2

sured at two periods, 100 and 50 seconds. Moments based on the amplitudes at 50 s period are lower on the average than those of the 100 s. Taken average values the lowest moment is that of NAT1, but the difference is so small that practically all moments can be say to be equal.

To examine the scatter of the data and the influence of the radiation pattern factor we have plotted in figure 9 the values of the spectral amplitudes corrected by spreading and attenuation versus distance. In the figure the curves corresponding to constant moment are shown. These have been calculated for a theoretical model with vertical strike-slip faulting at a surface focus (30 km) and corresponds to spectral amplitudes recorded at 45^{o} from the fault plane. Scatter of the observed spectral amplitudes amounts on the average to one order of magnitude. Spectral amplitudes at 50 s are more scattered than those at 100 s.

If moments are calculated from the spectral amplitudes at 100 s using the diagram of figure 9 prescinding of the focal mechanism, the average for each shock are in good agreement with the average values obtained from table 3 where all factors have been considered in the calculations

shock	M_o(calculated) 10^{24} dyne-cm	M_o(diagram) 10^{24} dyne-cm
AZOR	3.5	2.4
ALEU	1.3	2.4
NAT1	4.1	1.9
NAT2	3.9	3.3

Differences are within the range of error usually admitted for this parameter. Provided that stations are not near a

nodal plane and that mechanisms have large strike-slip component of motion curves of figure 9 should give on the average sufficiently good estimates of the seismic moment.

Fault lengths have been calculated for the four shocks from the directivity function according to equation (2). The rupture velocity has been taken as 1.5 km/sec. An example of the directivity function for NAT2 calculated from the spectra of HGLP stations of KON and TLO is shown in figure 10. Values of b are given in table 4. The rupture velocity has been chosen to keep the fault dimensions in agreement with the results from body waves. However, increasing v to 2 km/sec, a more commonly accepted value, increases b in only about 10 km.

Spectra of Shear Waves

Analysis of body waves has been limited to only two shocks and the study of S waves. Only for ALEU and NAT2 the S wave pulses were sufficiently clear. Spectra are shown in figures 11, 12, 13 and 14. Data from HGLP stations have been found very useful, since long period S waves are there usually well recorded. The spectral level at low frequencies are in general well defined. Corner frequencies are less reliable, with a certain amount of uncertainty with respect to the position of the point of intersection of the constant level Ω_o with the sloping line of amplitude with frequency.

Values for seismic moment and radius of the circular fracture have been calculated using equations (5) and (6). Results are shown in table 5. Moments are similar to those found from Rayleigh waves spectra, though somewhat lower. Figure 15 shows the spectral amplitudes distance relation with

TABLE 4

Length of fault from directivity of Rayleigh waves.

Shock	Stations	b (Km)
AZOR	BUL / LON (WWSSN)	27
ALEU	ALQ / NOR (WWSSN)	54
	"	47
NAT1	AQU / BEC (WWSSN)	43
NAT2	KON / TLO (HGLP)	31
	KON / ALQ (HGLP)	(68)
	TLO / ALQ (HGLP)	42

TABLE 5

Seismic moments and diameter of fault from shear waves.

STATION	R (km)	$_{o}$(M-6)	$M_o 10^{24}$ dyne-cm)	f_o(cps)	2r(km)
ALEU					
ALQ-HGLP(ANAL)-(03)	6058	0.31	0.2	0.092	15.4
FBK-HGLP(ANAL)-(03)	2415	-	-	0.108	14.2
-(02)	"	-	-	0.045	31.0
CGH-HGLP(DTS)-(A3)	7858	0.3	0.8	0.039	36.3
COL-WWSSN -(05)	2427	2.7	0.3	0.051	27.7
-(06)	"	1.5		0.082	17.3
COR-WWSSN -(06)	4266	1.3	0.2	0.051	27.7
DUG-WWSSN -(06)	5253	0.26	0.2	0.082	17.3
NAT2					
ALQ-HGLP(DTS)-(A2)	6041	1.62	1.6	0.078	13.0
KON-HGLP(ANAL)-(05)	4672	0.57	0.4	0.082	17.3

curves of constant moment. Curves have been calculated without the radiation pattern term, taking instead the mean value of the radiation. The spread of the observed spectral amplitudes is much less than for Rayleigh wave data (figure 9). The correction for the radiation pattern is in this case not very important and values of moments can be calculated with sufficient approximation without that term. Comparing the diameter obtained for the circular crack with the length of the rectangular fault used in the directivity calculations, it corresponds to the equivalent dimension for equal area correspondance taking a fault width of 2/3 the fault length.

Seismic energy, stress drop and average stress

To complete the determination of source parameters the radiated seismic energy has been calculated using the equations (4) and (10) from the values of magnitude. Surface wave magnitudes have been calculated from amplitude readings at several stations and by means of equation (3). Results are shown in table 6. For body wave magnitude that given by USCGS has been adopted. Energies calculated from m_b are lower than those from M_s. This is due to the fact that m_b (CGS) is lower than the body wave magnitude corresponding to our values of M_s according to the relation

$$m_b = 2.5 + 0.63\, M_s \qquad (21)$$

Stress drops $\Delta\sigma$ have been calculated from Rayleigh wave data using equation (17) and from S wave data using (18). Results are shown in table 6. Stress drops are rather low, specially for ALEU (R) due to the high value obtained for b.

TABLE 6

Source parameters.

SHOCK	M_s, m_b	E_s	M_o	b,2r	A	$\Delta\sigma$	$\eta\bar{\sigma}$	$\bar{w}$
		10^{19} ergs	10^{24} dyne-cm	km	km^2	bars	bars	cm
Rayleigh waves								
AZOR	5.5	11	3.5	27	243	1.1	10.4	4.3
ALEU	5.5	11	1.3	51	867	.06	27.9	0.4
NAT1	5.0	2	4.1	43	616	0.3	1.6	2.0
NAT2	5.4	9	3.9	36	432	0.5	7.6	2.7
S - waves								
ALEU	5.5	1	0.3	23	416	0.1	11	0.2
NAT2	5.5	1	1	15	176	1.2	3.3	2.0

In figure 16 seismic moments have been plotted versus fault area. Curves of constant stress drop have been also drawn for Brune's circular crack model. The stress drops found here vary between 0.1 and 1 bar and are lower by an order of magnitude than tne expected from Brune's model. In the same figure we have plotted values determined by other authors using the same methods as here (see table 7). We find in these values again a good agreement between calculations using Rayleigh and S waves. Stress drops are between 0.1 and 10 bars and also a little lower than the expected from the model.

The ratios of the seismic energy to moment have been interpreted as giving a measurement of the apparent average shear stress on the fault zone. The values obtained here vary from 1 to 30 bars. Since η must be less than unity, these are minimum estimates of the average stress. The order of magnitude obtained agrees with that generally accepted for the strength of the earth crust under horizontal shear stress (Chinnery, 1964). Randall's contention that this ratio actually represents $1/2\ \Delta\sigma\eta$ does not agree with our results where its values are higher than those obtained for $\Delta\sigma$ from the moment and dimensions of the fault. Low stresses are expected at the zone of oceanic ridges, which will explain the values found for AZOR, NAT1 and NAT2. The stress for ALEU is higher, but due to the uncertainties intrinsic to this type of determinations it is hard to say if this difference is significant.

Accepting the interpretation given to the values of the stress drop and average stress, the relation between them will give a fractional stress drop of 10% for seismic

TABLE 7

Source parameters from other authors.

EVENT	M_S, M_L	M_o	b, 2r	A	$\Delta\sigma$	Source
		10^{24} dyne-cm	km	km^2	bars	
Rayleigh waves						
17-11-63	6.5	38	27	243	11.7	Atlantic; Udías (1971)
17- 5-64	5.7	3.2	29	290	1.5	" Rodriguez-P and Udías (1972)
4- 7-66	5.3	2	18	108	2.1	" Udías (1971)
29- 6-66	4.9	0.6	30	400	0.1	California; Wyss and Brune (1968)
S waves						
24- 7-47	5.0	0.10	3.8	11	7	California; Thatcher and Hanks (1972)
28- 7-50	5.4	0.82	8	50	5.7	" " "
25- 7-52	5.7	5.0	14	153	6.6	" " "
25- 4-55	5.2	0.61	19.8	308	0.3	" " "
28- 6-66	4.7	0.81	11.4	102	1.9	" " "
9- 4-68	6.4	66.0	46	1662	2.4	" Hanks and Wyss (1972)
9- 2-71	6.6	70.0	17	570	14	" Wyss and Hanks (1972)

efficiency equal to unity. A similar result was found by Wyss and Brune (1968) for earthquakes in the California Nevada region.

Average dislocations have been determined from equation (14) and (15). Values range from 0.2 to 4 cm. These values agree with those found by other authors for shocks of similar magnitude.

CONCLUSIONS

Records from high-gain long-period (HGLP) stations have been found useful in the analysis of source parameters of earthquakes of magnitude about 5. For this magnitude level and distances between 2000 and 8000 km Rayleigh waves are well recorded and in many cases clear S wave pulses can be found. These data is well suited for determination of source parameters from spectra of both types of waves.

Independent determinations of source parameters from Rayleigh and shear wave data show good agreement. In each case one can find independent estimates of seismic energy, moment and dimensions of the fault and from these derive values for stress drop, apparent average stress and average dislocation.

For surface shocks of magnitude between 5 and 6 we have found consistently low stress drops between 0.1 and 1 bars which compared with the apparent average stress give maximum fractional drops of stress of 10%. Faults areas are between 200 and 800 km^2 and total seismic moments of the order of 10^{24} dynes-cm.

REFERENCES

Aki, K. 1967. Scaling law of seismic spectrum. J. Geophys. Res., 72, 1217-1231.

Aki, K. 1972. Earthquake mechanism. The Upper Mantle; edited by A.R. Ritsema. Elsevier. 423-446.

Ben Menahen, A. 1961. Radiation of seismic surface waves from finite moving sources. Bull. Seis. Soc. Am.,51, 401-435.

Ben Menahen, A., S.W. Smith and T.L. Teng, 1965. A procedure for source studies from spectrums of long-period seismic body waves. Bull. Seis. Soc. Am., 55,203-235.

Ben Menahen, A., M. Rosenman and D.G. Harkrider, 1970. Fast evaluation of source parameters from isolated surface waves signals. Bull. Seis. Soc. Am.,60,1337-1387.

Brune, J.N., 1970. Tectonic stress and the spectra of seismic shear waves from earthquakes. J.Geophys. Res., 75, 4997-5009.

Brune, J.N., 1971. Correction. J. Geophys. Res., 76, 5002.

Brune, J.N. and C.R. Allen, 1967. A low stress drop low magnitude earthquake with surface faulting, the Imperial Valley California earthquake of March 4, 1966. Bull. Seis. Soc. Am., 57, 501-514.

Chinnery, M.A., 1964. The strength of the Earth's crust under horizontal shear stress. J.Geophys. Res., 69, 2085-2089.

Dahlen, F.A., 1974. On the ratio of P-wave to S-wave corner frequencies for shallow earthquakes sources. Bull Seis. Soc. Am., 66, 1159-1180.

Hanks, T.C. and M. Wyss, 1972. The use of body-wave spectra in the determination of seismic source parameters. Bull. Seis. Soc. Am., 62, 561-589.

Randall, M.J., 1972. Stress drop and the ratio of seismic energy to moment. J. Geophys. Res. 77, 969-970.

Richter, C.F., 1958. Elementary seismology. Freeman, San Francisco.

Rodriguez-Portugal, C. and A. Udías, 1972. Estudio del mecanismo y determinación de los parametros dinámicos del foco del terremoto de Azores del 17 de Mayo de 1964. Rev. de Geofísica, XXXI, 63-86.

Savino, J.N., A.J. Murphy, J.M. Rynn, R. Tatham, L.R. Sykes, G.L. Choy and K. McCamy, 1972. Results from the high-gain long-period seismograph experiment. Geophys. J.R. astr. Soc., 31, 179-203.

Stauder, W., 1968. Mechanism of the Rat Islands earthquake sequence of February 4, 1965 with relation to island arc and seafloor spreading. J. Geophys. Res., 73, 3948-3858.

Tatcher, W. and T.C. Hanks, 1973. Source parameters of Southern California earthquakes. J. Geophys. Res., 78, 8547-8576.

Udías, A., 1971. Source parameters of earthquakes from spectra of Rayleigh waves. Geophys. J.R. astr. Soc. 22, 353-376.

Wyss, M. and J.N. Brune, 1968. Seismic moment, stress and source dimensions for earthquakes in the California-Nevada region. J. Geophys. Res., 73, 4681-4694.

Wyss, M. and T.C. Hanks, 1972. The source parameters of the San Fernando earthquake inferred from teleseismic body waves. Bull. Seis. Soc. Am., 62, 591-602.

LIST OF FIGURES

13. Spectrum of shear waves at the WWSSN station of COR for the 3 Jan 1972 (ALEU) earthquake.

14. Spectrum of shear waves at the HGLP (digital data) station of ALQ, for the 6 June 1972 (NAT2) earthquake.

15. Relation between spectral amplitudes corrected for attenuation and spreading distance for shear waves. Curves of constant seismic moment are given in dyne-cm.

16. Relation between seismic moment and fault area. Circles (open Rayleigh and black shear wave data) from table 6 (this study). Triangles (open Rayleigh, and black shear wave data) from table 7. Curves of constant stress drop in bars.

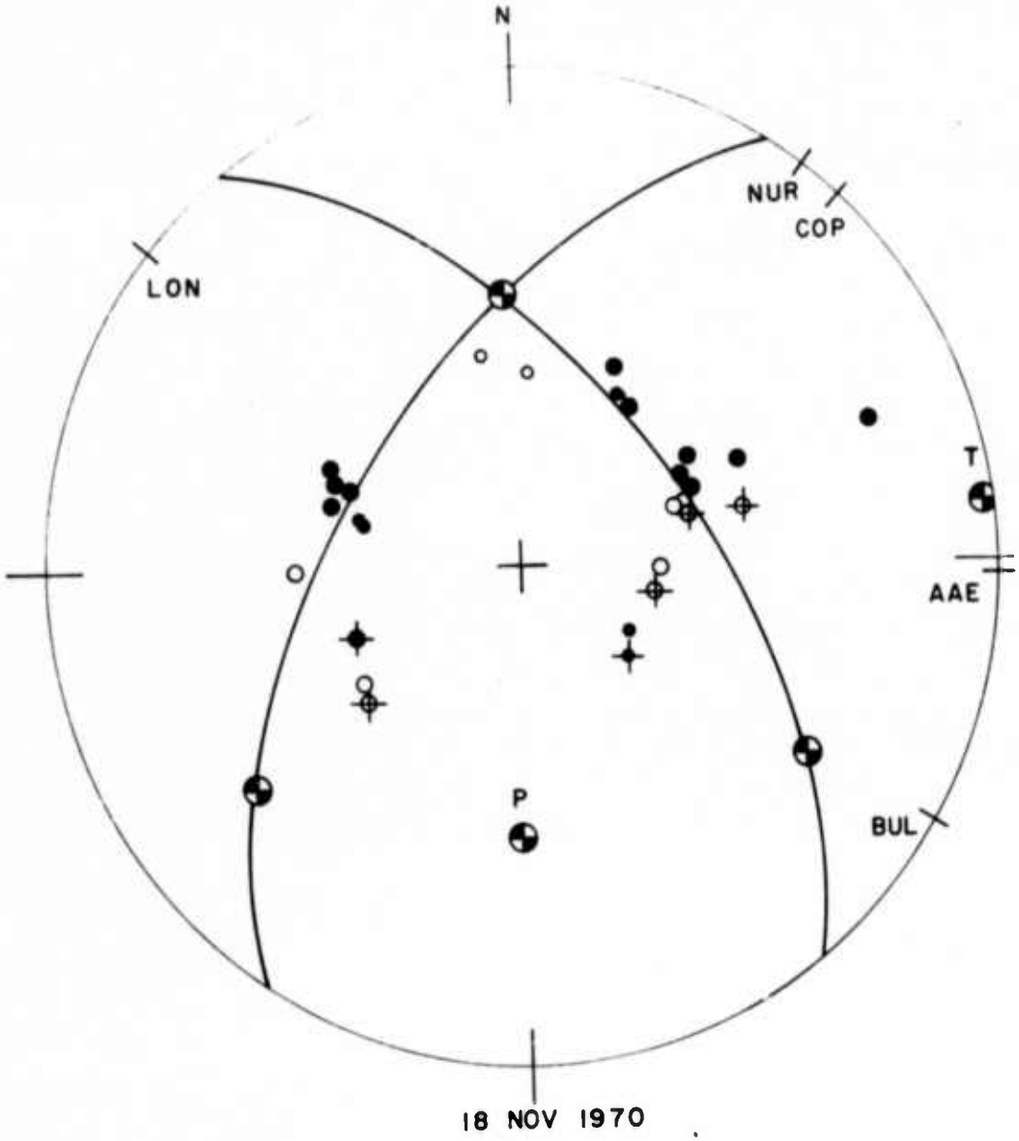

Figure 1. Focal mechanism solution for the Azores earthquake of 18 Nov 1970 (AZOR). Shown the positions of stations used in Rayleigh wave analysis.

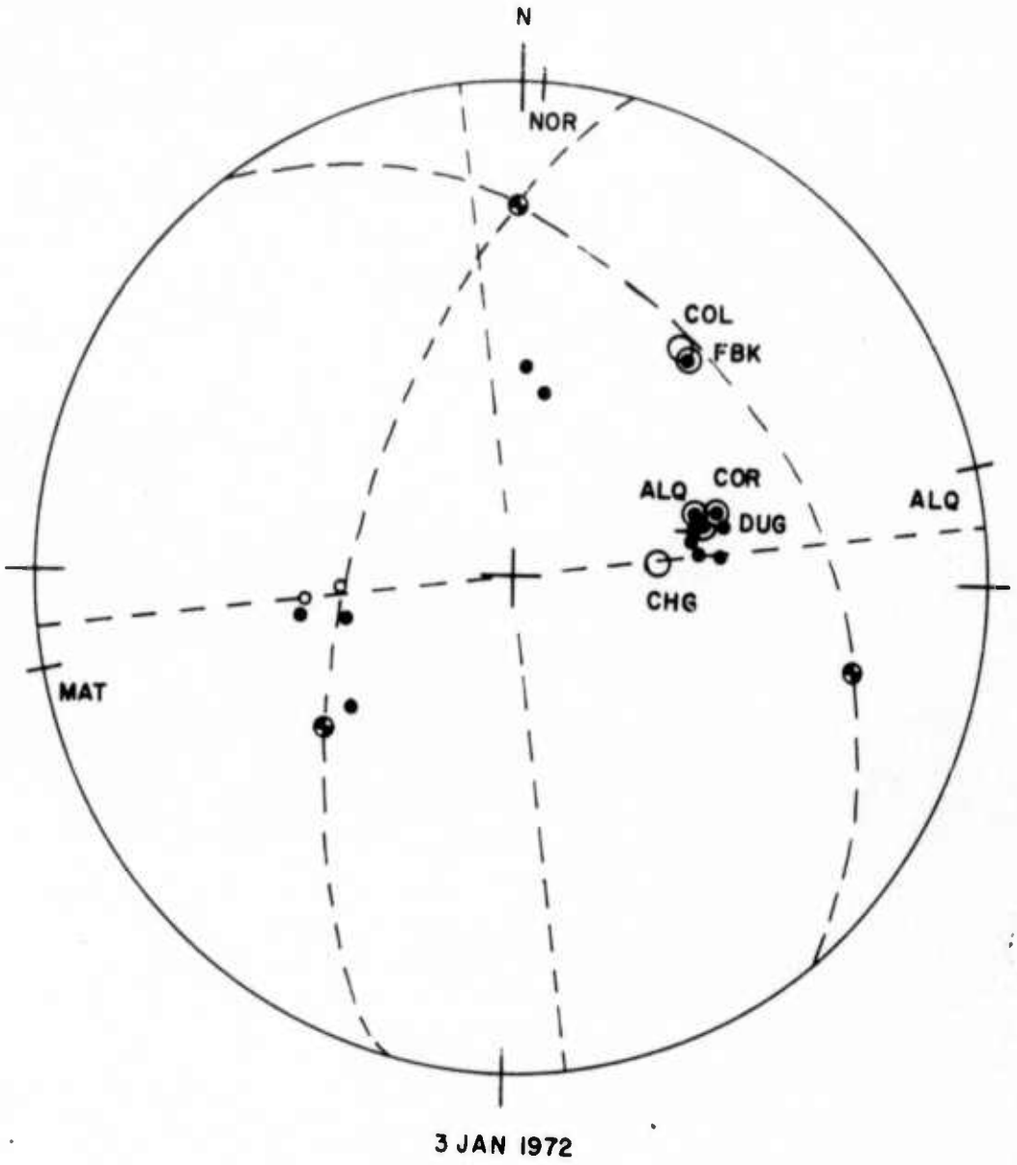

Figure 2. Focal mechanism solution for the Aleutian Islands earthquake of 3 Jan 1972 (ALEU). Shown the positions of the stations used in the Rayleigh wave (rim) and shear wave (inside) analysis.

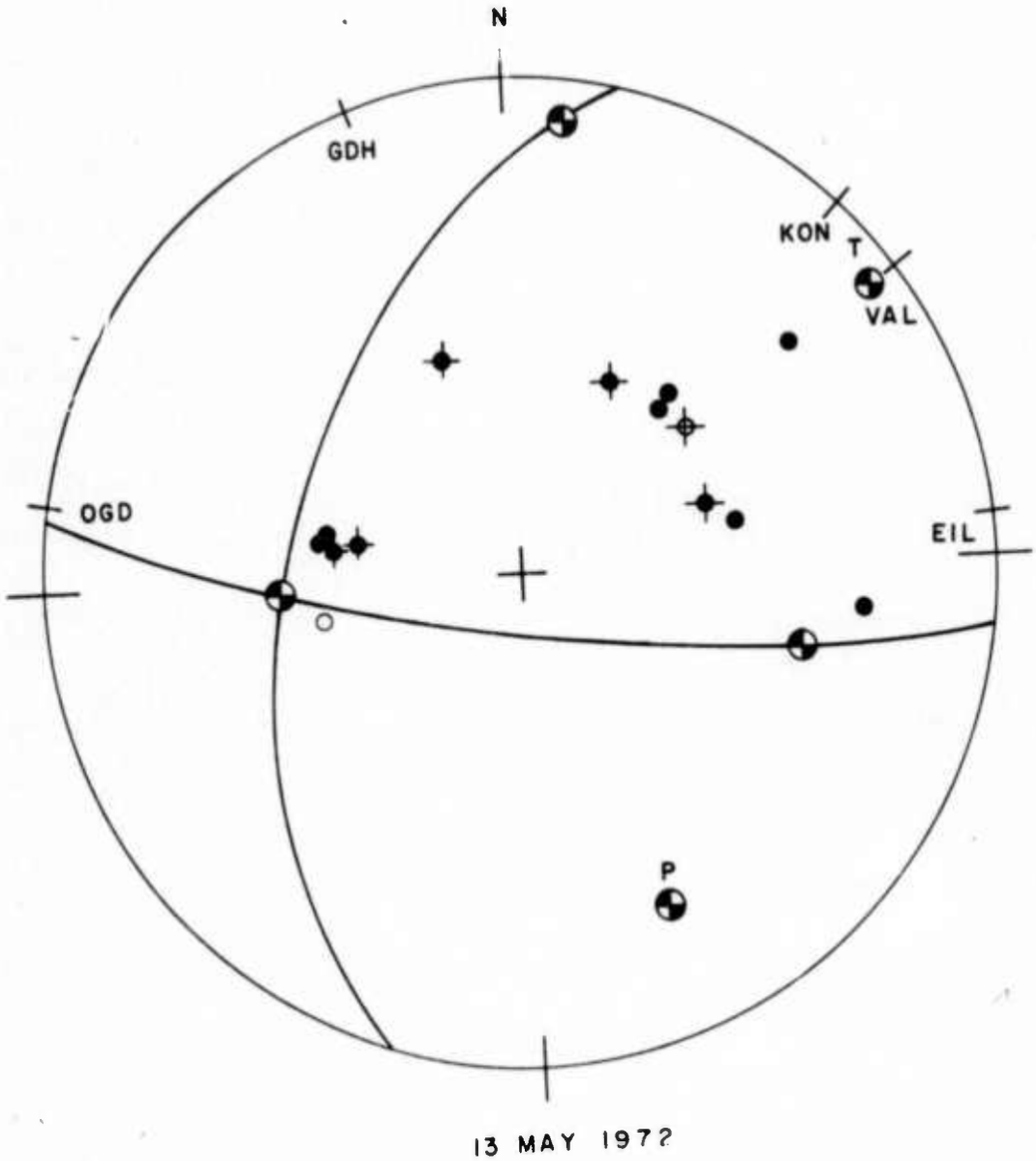

Figure 3. Focal mechanism solution for the North Atlantic earthquake of 6 Jun 1972 (NAT1). Shown the position of the stations used in Rayleigh wave anelysis.

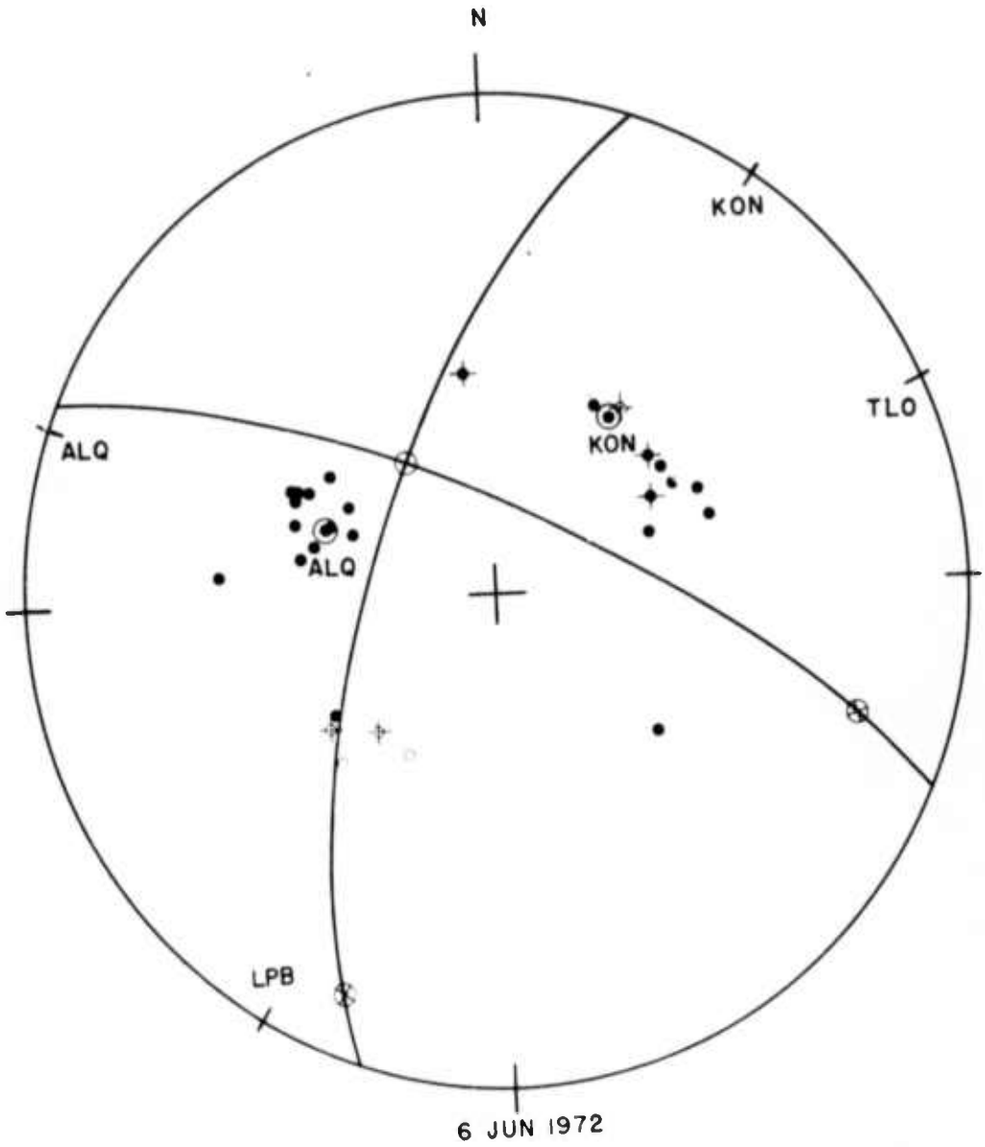

Figure 4. Focal mechanism solution for the North Atlantic earthquake of 6 Jun 1972 (NAT2). Shown the position of the stations used in the Rayleigh wave (rim) and shear wave (inside) analysis.

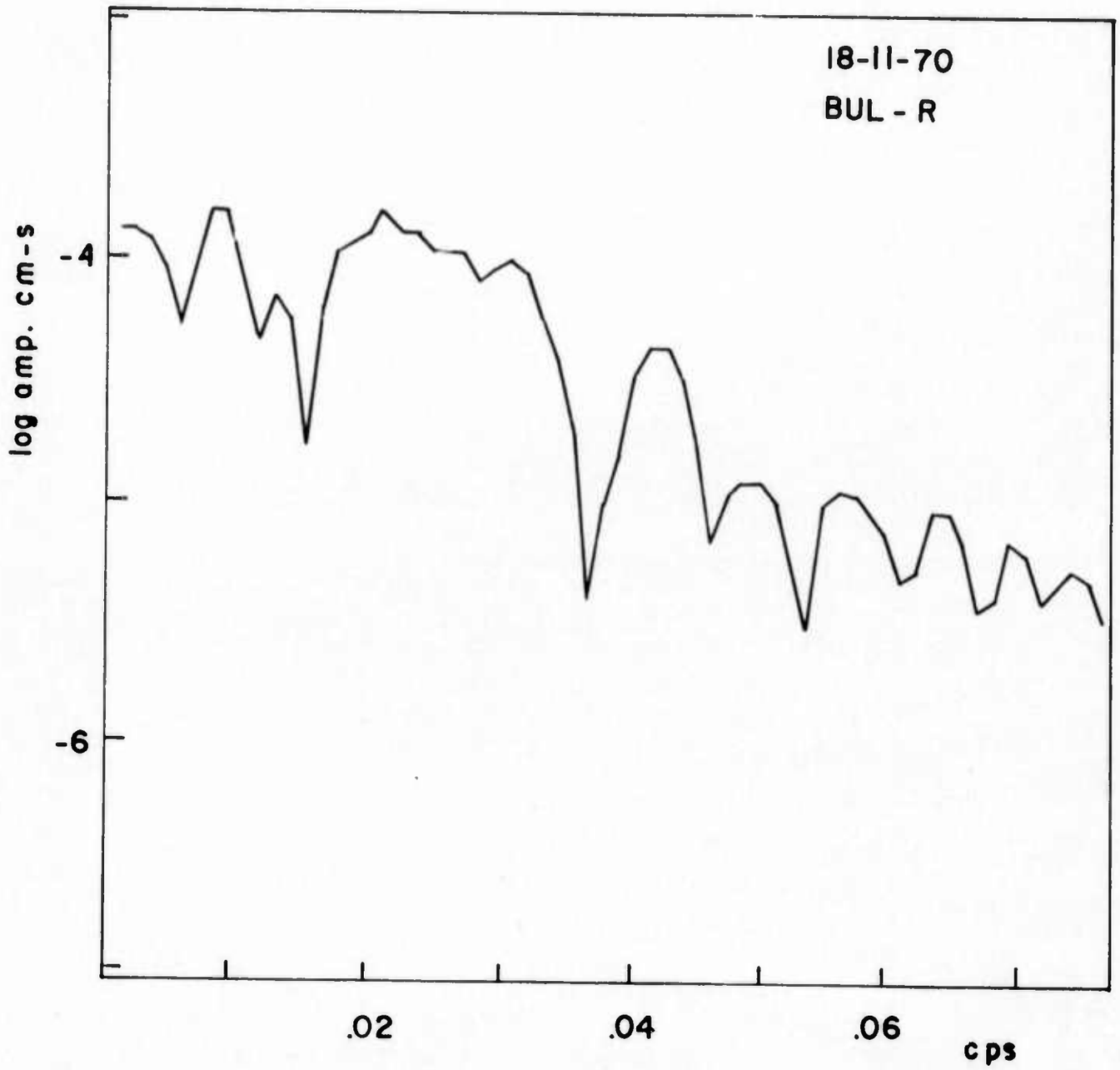

Figure 5. Spectrum of Rayleigh wave at WWSSN station of BUL for the 18 Nov 1970 (AZOR) earthquake.

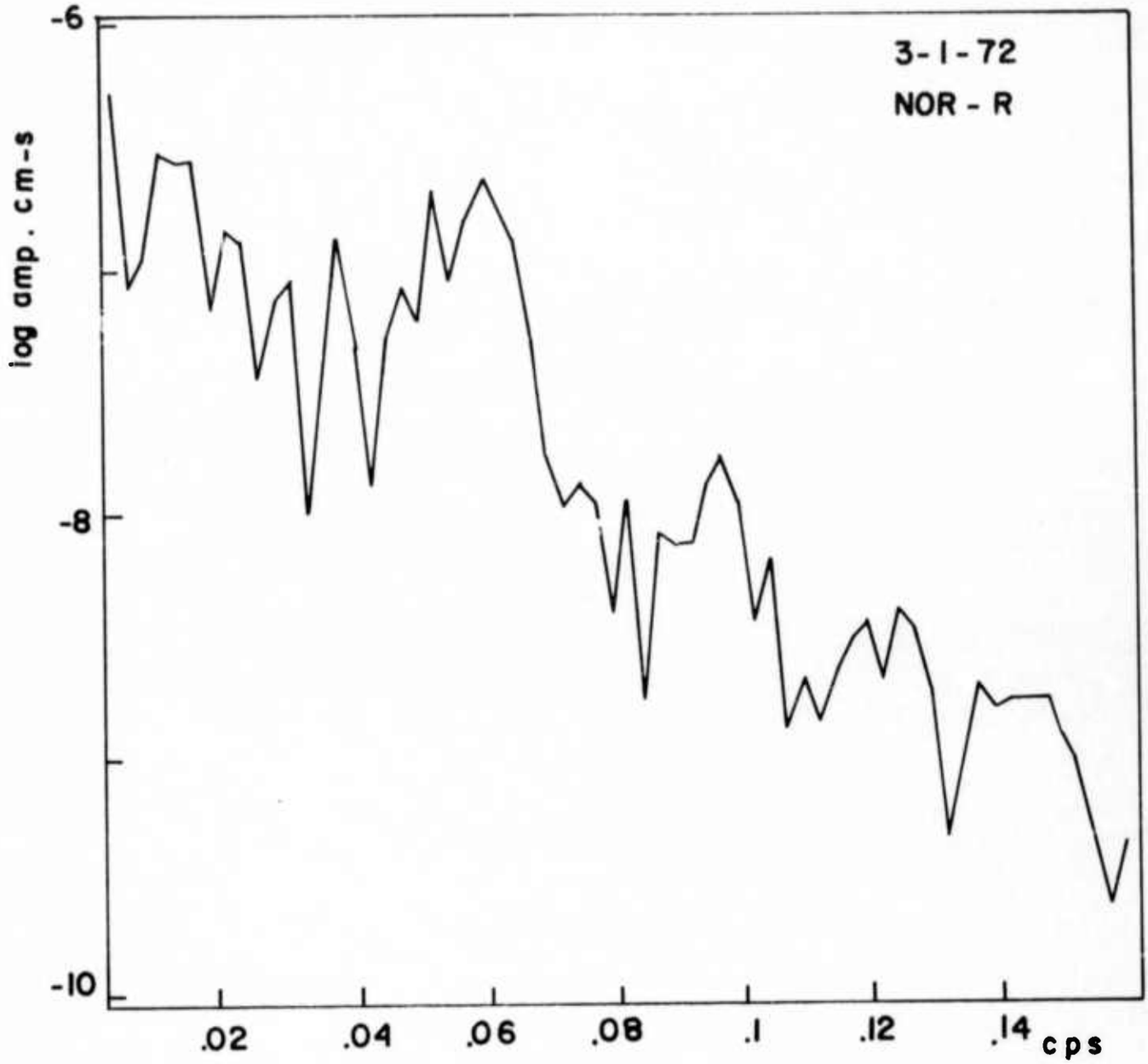

Figure 6. Spectrum of Rayleigh wave at the WWSSN station of NOR for the 3 Jan 1972 (ALEU) earthquake.

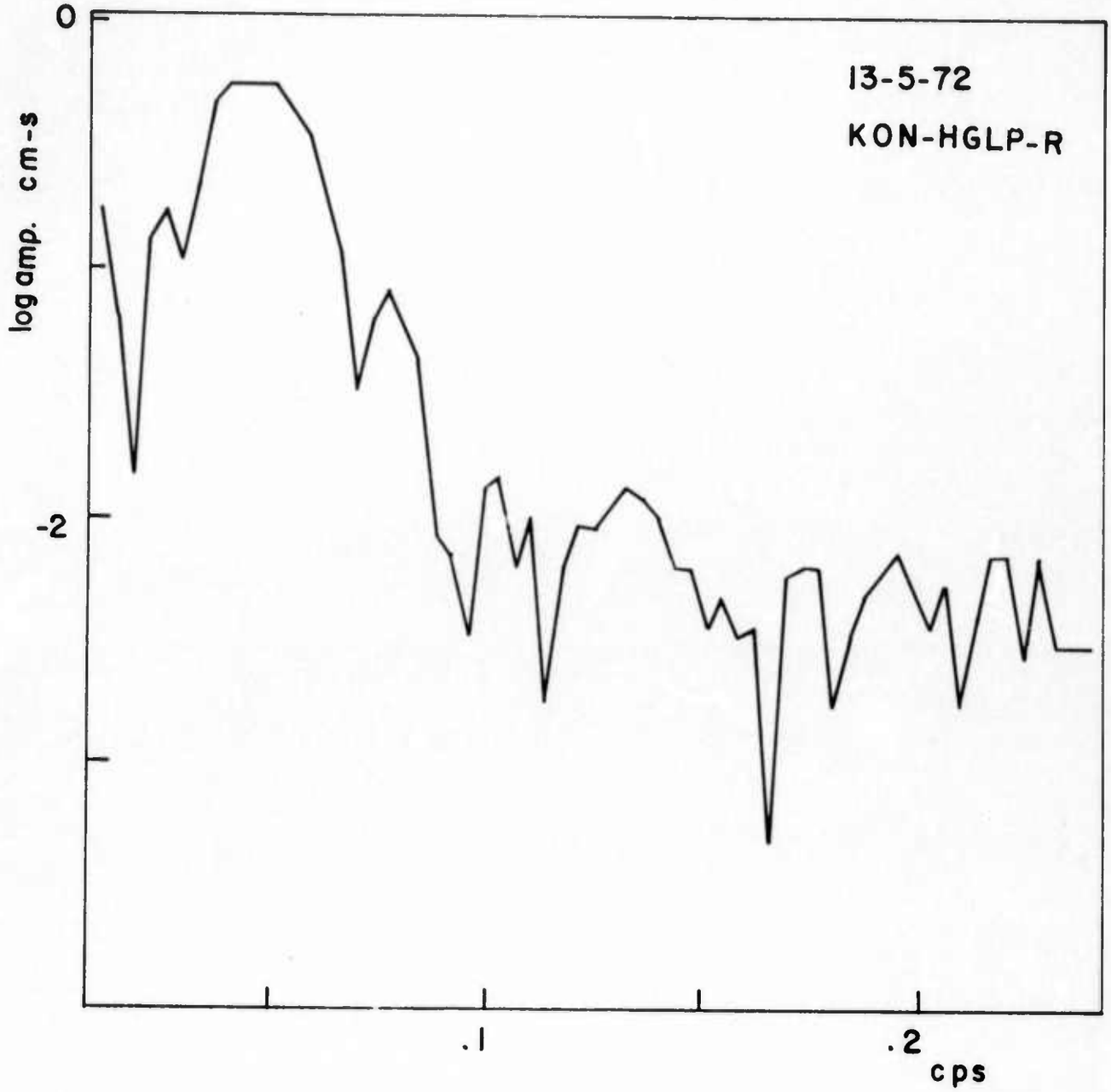

Figure 7. Spectrum of Rayleigh wave at the HGLP station of KON for the 13 May 1972 (NAT1) earthquake.

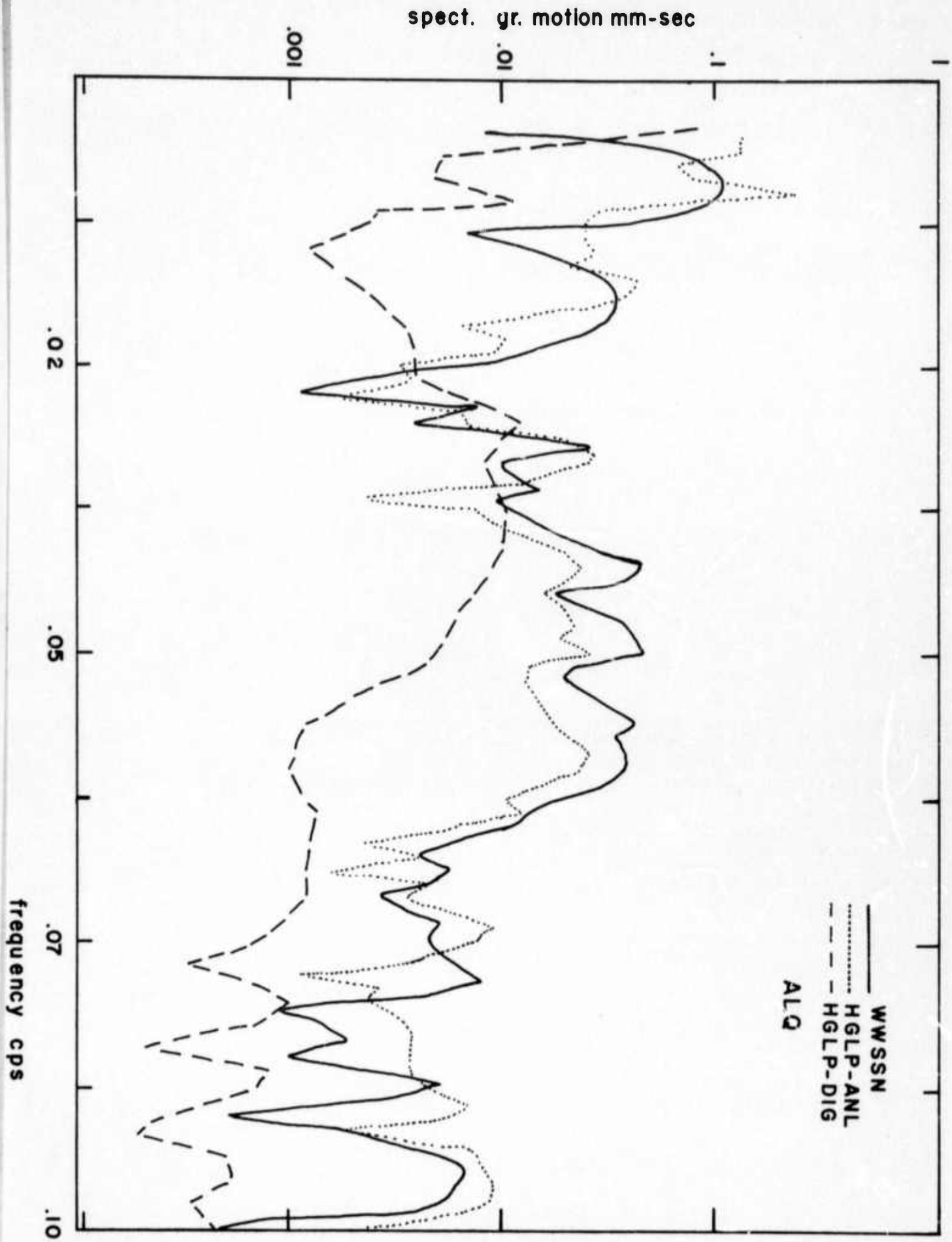

Figure 8. Spectra of Rayleigh wave for the HGLP (digital and analog records) and WWSSN stations at ALQ for the 6 Jun 1972 (NAT2) earthquake.

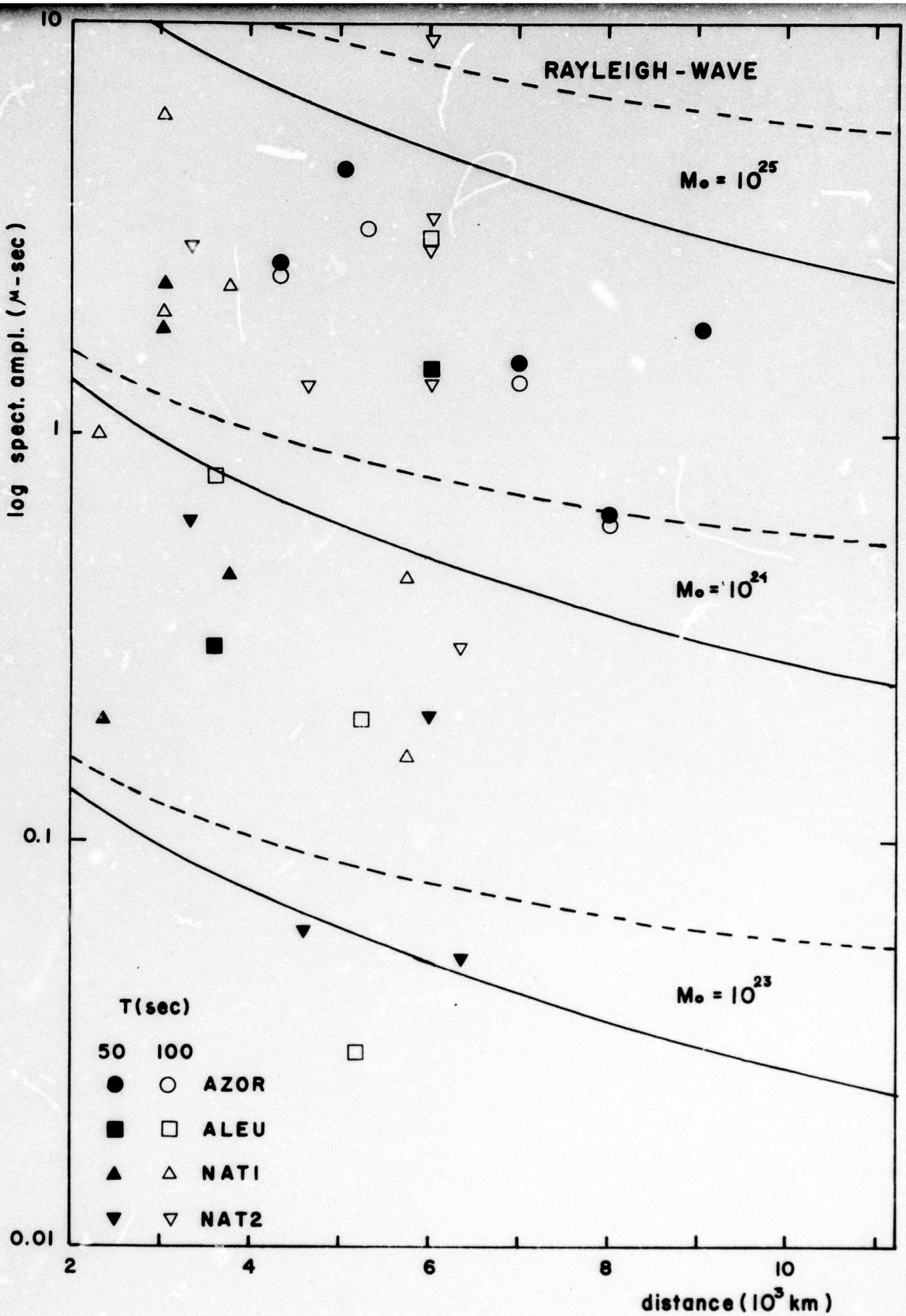

Figure 9. Relation between the spectral amplitudes corrected for attenuation and spreading and distance for Rayleigh waves. Curves of constant seismic moment given in dyne-cm.

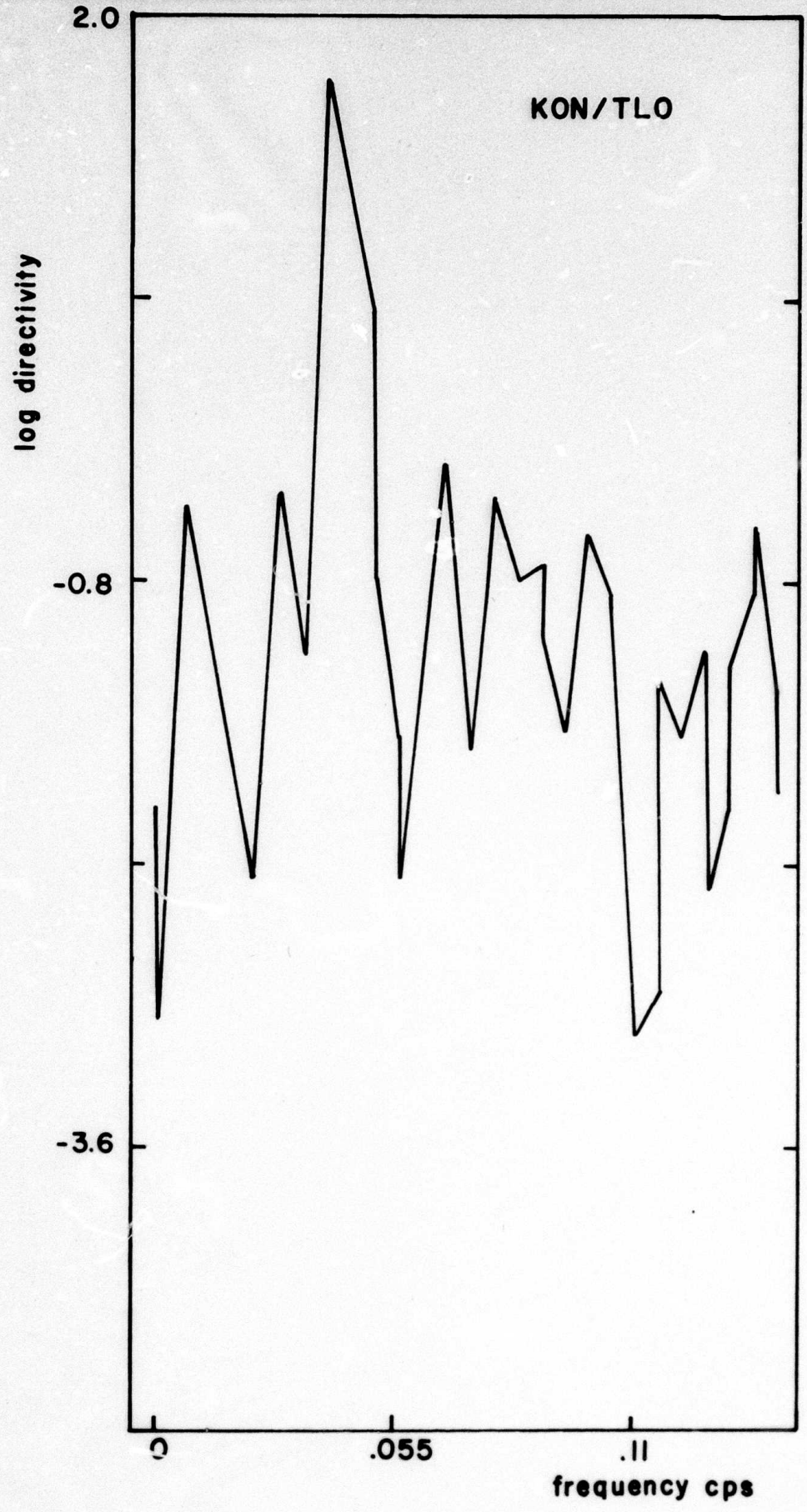

Figure 10. Directivity function of Rayleigh waves for the HGLP stations of KON and TLO.

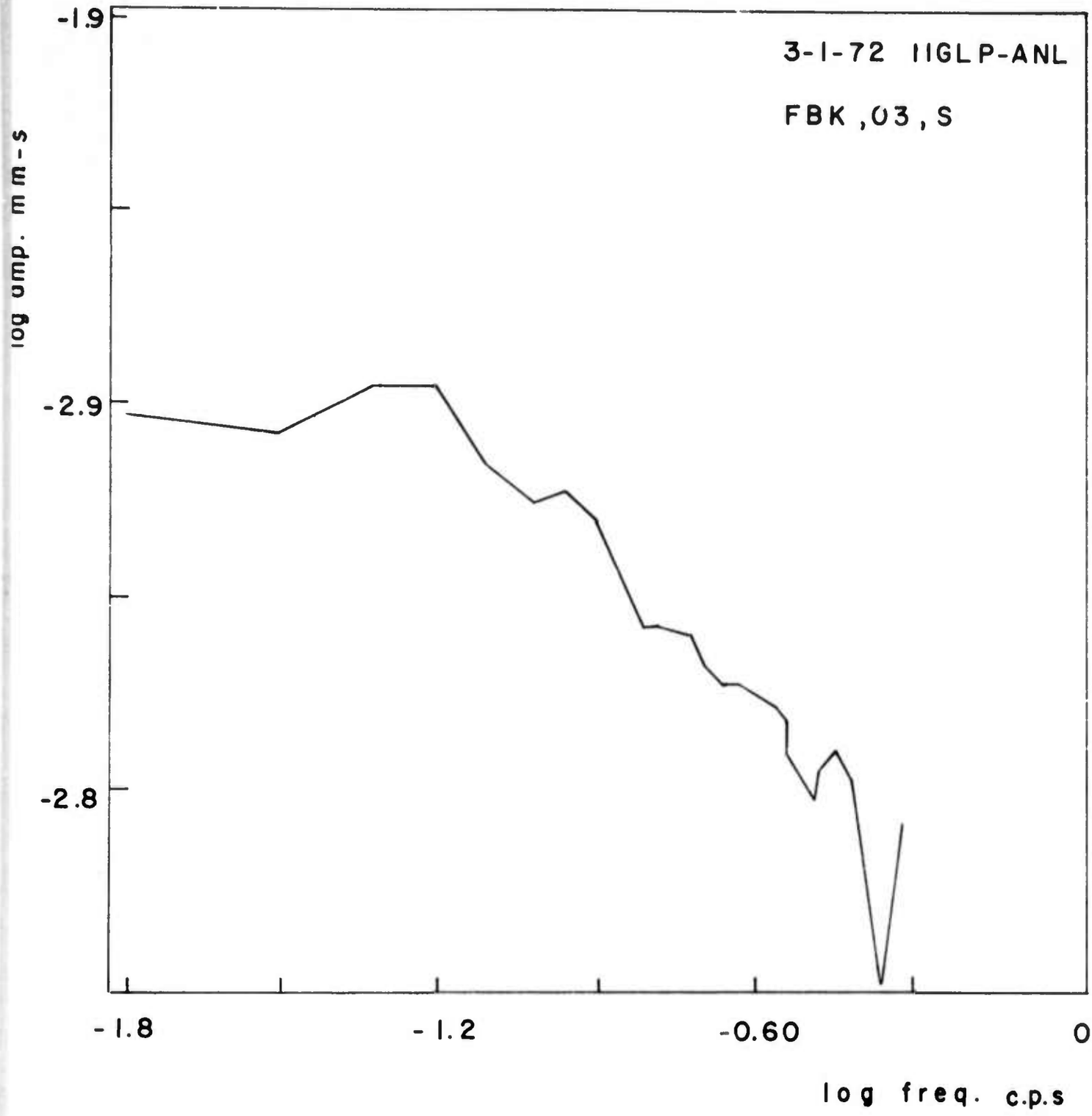

Figure 11. Spectrum of shear waves at the HGLP station of FBK for the 3 Jan 1972 (ALEU) earthquake.

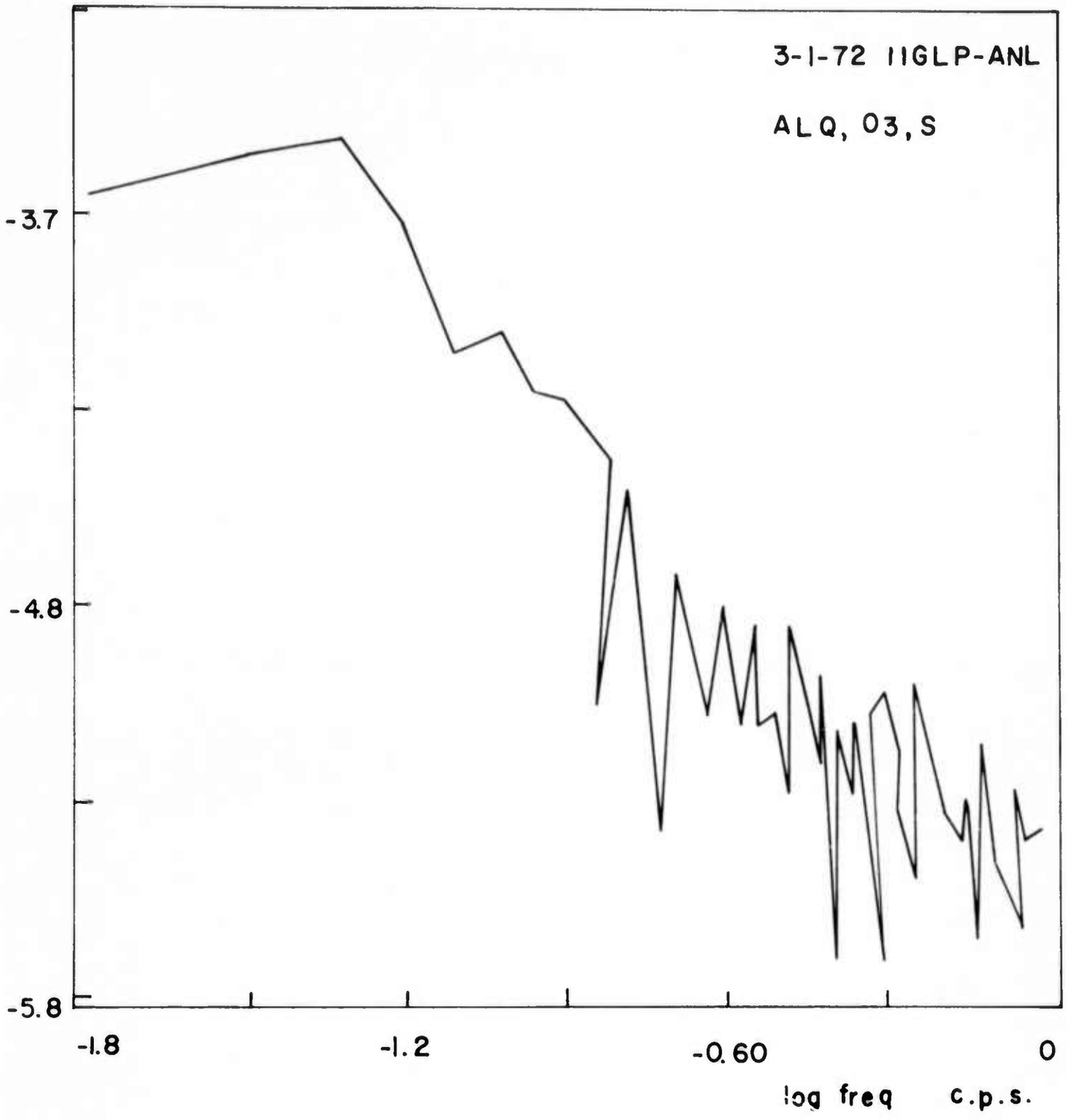

Figure 12. Spectrum of shear waves at HGLP station of ALQ for the 3 Jan 1972 (ALEU) earthquake.

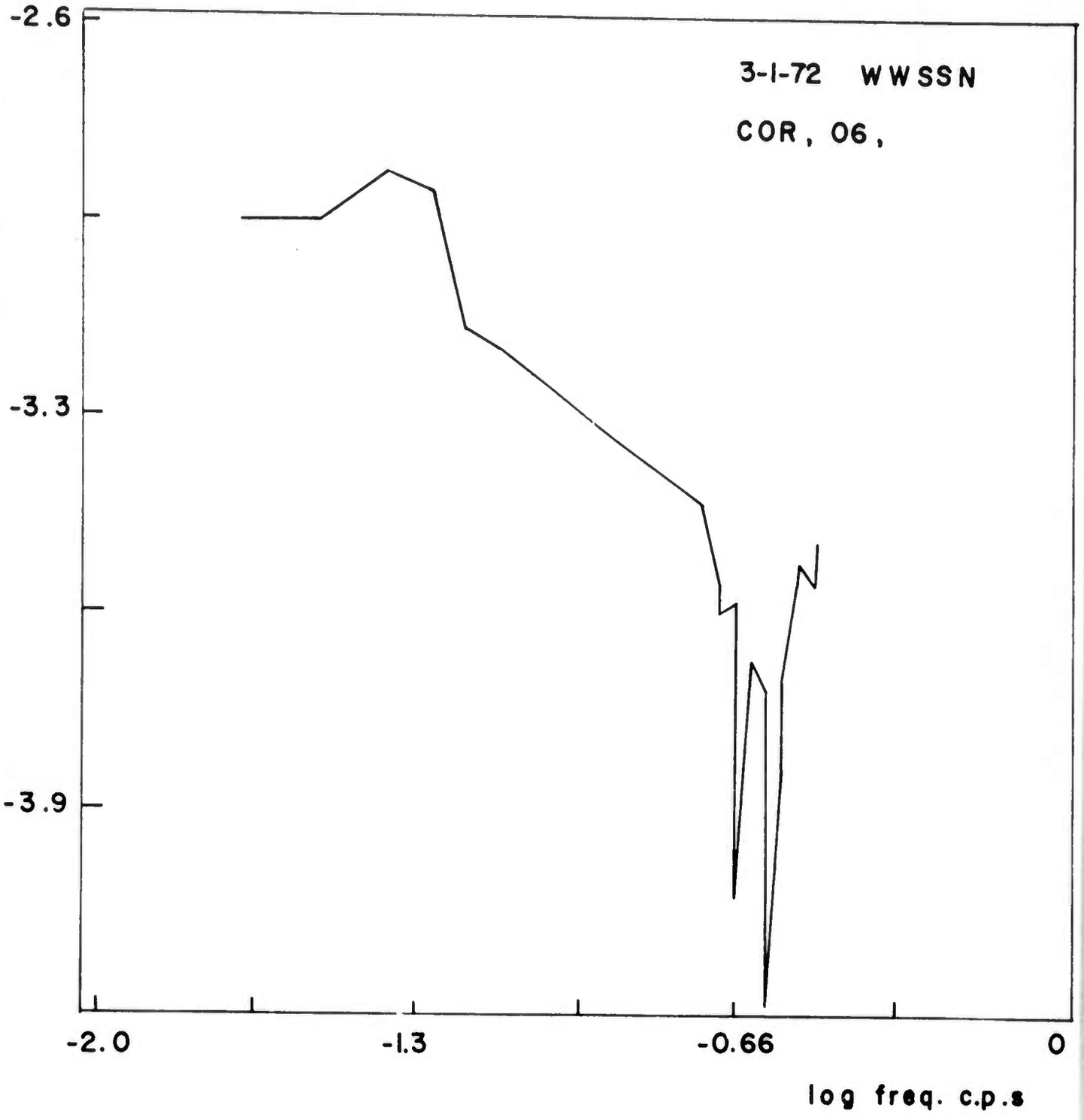

Figure 13. Spectrum of shear waves at the WWSSN station of COR for the 3 Jan 1972 (ALEU) earthquake.

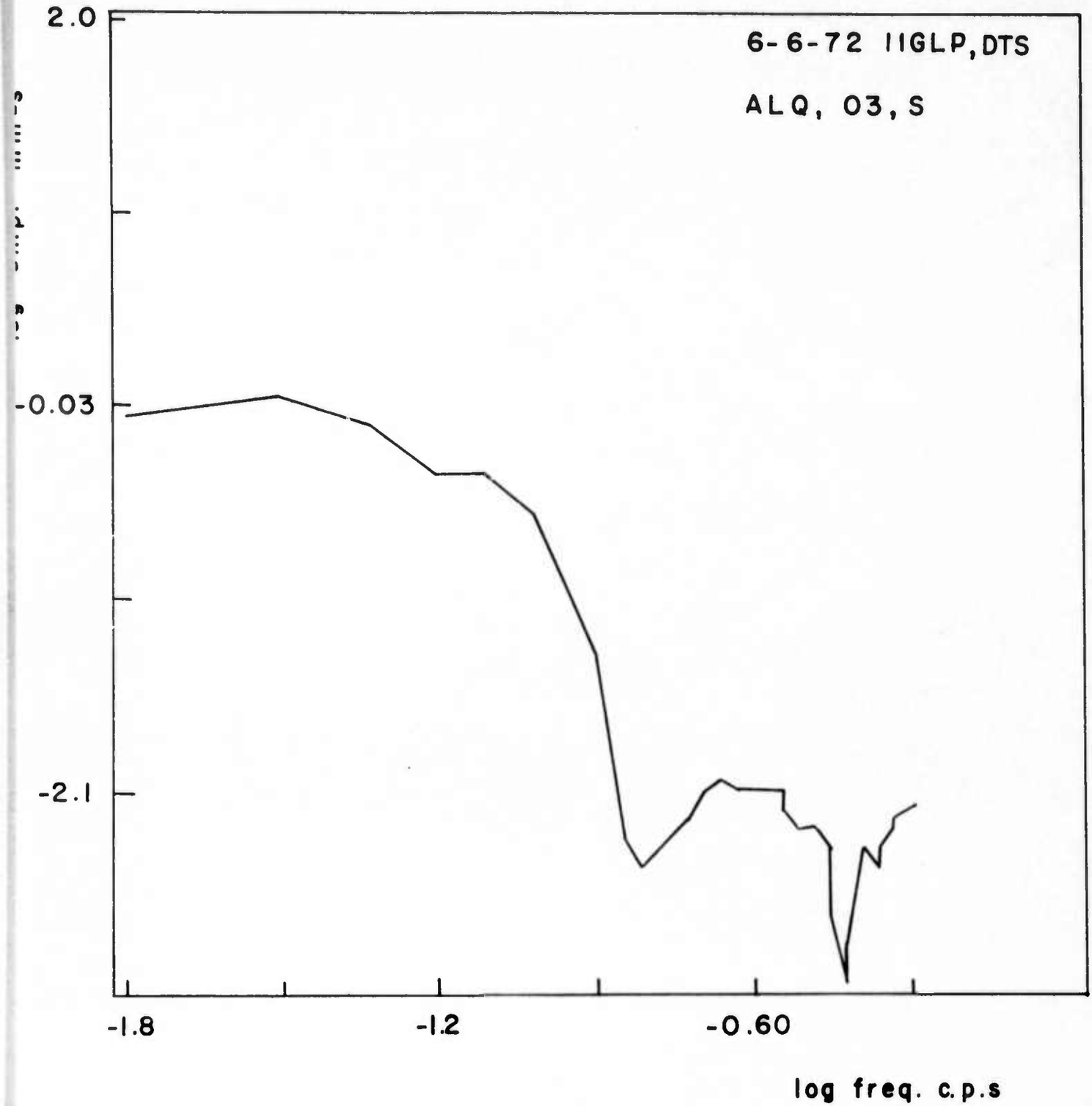

Figure 14. Spectrum of shear waves at the HGLP (digital data) station of ALQ, for the 6 June 1972 (NAT2) earthquake.

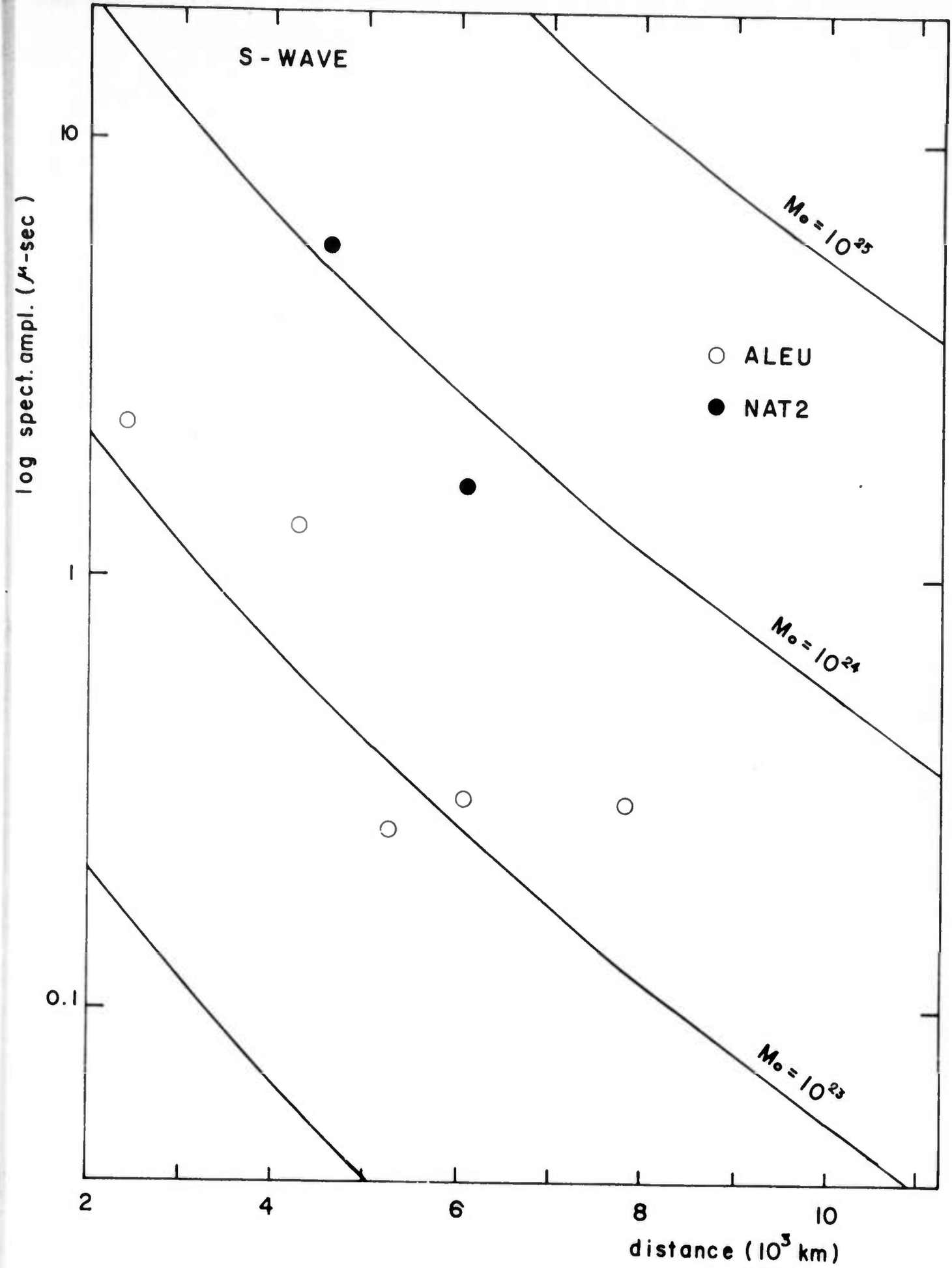

Figure 15. Relation between spectral amplitudes corrected for attenuation and spreading distance for sheer weves. Curves of constant seismic moment ere given in dyne-cm.

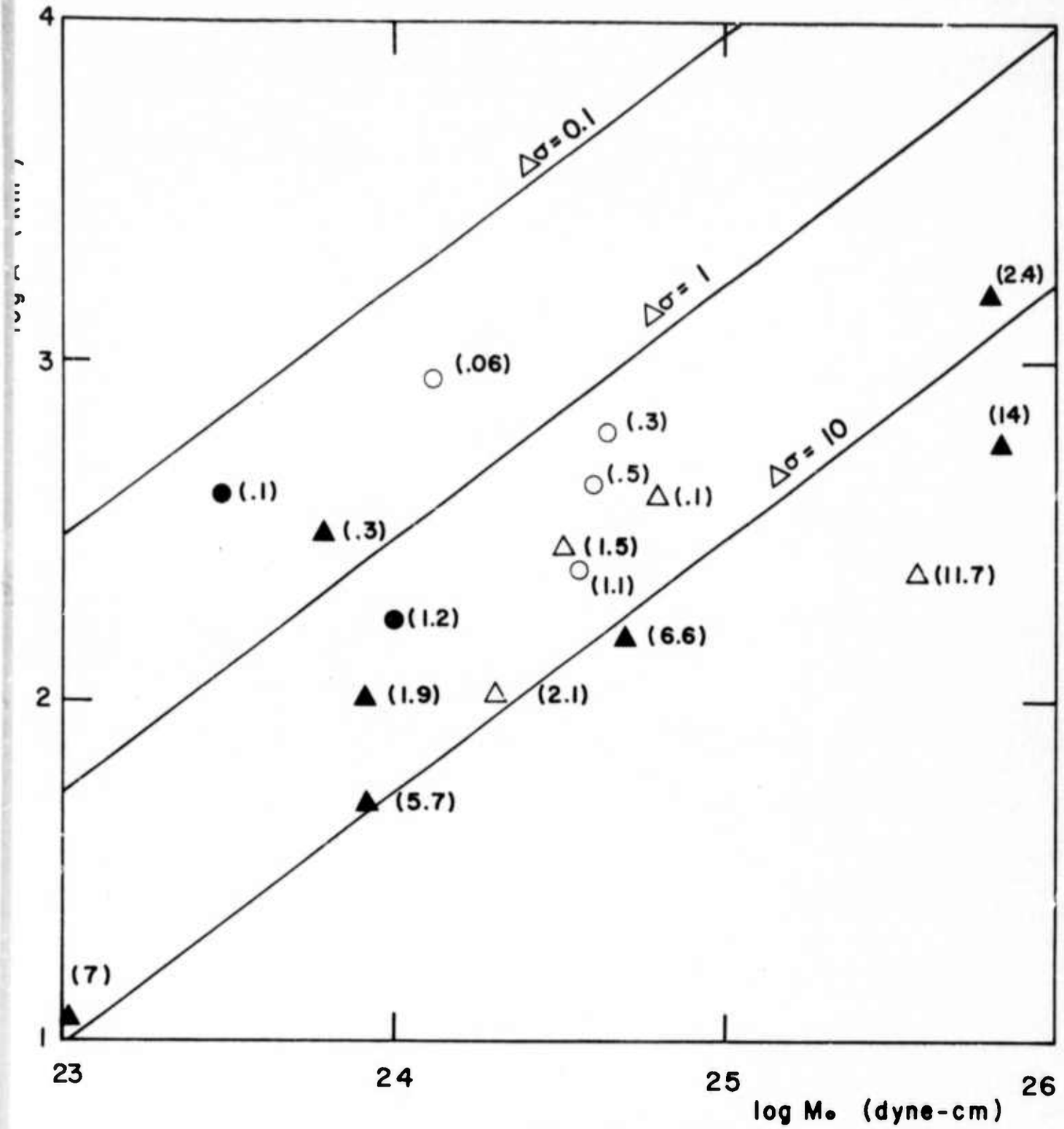

Figure 16. Relation between seismic moment and fault area. Circles (open Rayleigh and black shear wave data) from table 6 (this study). Triangles (open Rayleigh, and Black shear wave data) from teble 7. Curves of constant stress drop in bars.

ATTENUATION OF SEISMIC WAVES DETERMINED FROM HIGH-GAIN LONG-PERIOD STATIONS

Alfonso López-Arroyo and Julio Mezcua

Instituto Geográfico y Catastral

SUMMARY

A comparison is made of attenuation values obtained from data recorded by High Gain Long Period (HGLP) instruments and by stations of the Standard network. Attenuation refers to surface Rayleight waves generated by nuclear explosions and the frequency range considered extends from 0.1 to 0.01 Hz. For the distances involved in this study the use of such energy sources eliminates the uncertainites derived from lack sufficent knowledge of the radiation pattern, as this can be assumed to be spherically symmetrical. Attenuation coefficient for every frequency is given as the slope of a least square linear fitting of the spectral amplitud vs distance. Values obtained correspond to paths from Novaya Zemblya to Eastern USA, Canada and Europe. Results from HGLP show large scatter which reflect the insufficient control of the instrument response for the system. Had this problem been adequately solved, the HGLP data would have been far superior than standard data for the attenuation study, due to their larger dynamic range and readness to use on the computer.

INTRODUCTION

In the present study, we are concerned with the decreases in the amplitude density spectrum with distance. That is, we wish to know how the amplitude density at a given period (or frequency) decreases with increasing distance.

For the fundamental mode, a seismic surface disturbances, can be written as

$$u(x,t) = \frac{1}{2\pi} \int_{-\infty}^{\infty} \frac{A(\omega)}{\sqrt{\sin \theta}} \exp\left[-\frac{\omega t}{2Q}\right] \exp\left[i(\omega t + \phi)\right] d\omega \quad (1)$$

where

$$V(x,\omega) = \frac{A(\omega)}{\sqrt{\sin\theta}} \exp\left[-Kx\right]$$

and ϕ is a phase lag. The quantity V is the Fourier transform of u(x,t), and yields the amplitude density spectrum. A (W) represents the amplitude density function at the source, K the attenuation coeficient and θ the epicentral distance degrees.

In this form (Ewing et al., 1957) we can consider a train of travelling surface waves as formed by a synthesis of single harmonic waves. Let the suscript 1 refer to some reference distance, then

$$V(x_1,\omega) = \frac{A(\omega)}{\sqrt{\sin\theta_1}} \exp\left[-Kx_1\right]$$

and

$$\frac{V(x,\omega)}{V(x_1,\omega)} = \frac{\exp\left[-K(x-x_1)\right]}{\sqrt{\sin\theta/\sin\theta_1}}$$

Taking the logarithm of both sides of the preceding equation, gives

$$\ln V(x,\omega) - \ln V(x_1,\omega) = \frac{1}{2}\ln\sin\theta_1 - \frac{1}{2}\ln\sin\theta - KD \qquad (2)$$

where

$$D = X - X_1$$

Equation (2) can be written as

$$2\ln V(x,\omega) + \ln\sin\theta = C - 2KD \qquad (3)$$

For every given value of W, the terms on the left of equation (3) contain the amplitude density at a distance X, corrected for the effect of geometrical spreading over the surface of the spherical Earth. If the sum of the terms on the left is plotted against the independent variable D, the resulting straight line will have a slope equal to -2K and intercept of C. The equation (3) thus provides a method of determining K as a function of frequency

DATA ACQUISITION

By visual inspection of the high gain photographic records from the stations used in this paper we searched digital tapes from 1971 to 1974 and selected those with a clear train of surface waves. In this selection we eliminated the records with significant noise in the frequency range of our analysis, i.e., 0.01 - 0.1 Hz.

Once the data was preselected a computer program was used to get the digital data out from the tape. Again, a selection of those records without spurious spikes gave us the final data to be used in the present study. In this stage we used the programs HIGAN and EDITR from Lamont-Doherty Observatory to obtain the data off the tape.

In the case of WWSSN records, the normal procedure of digitizing 70 mm films provided by the NOAA, was used with a digitizing interval of 1 second.

To verify the digital data both in the Standard and HGLP records we developed a computer program to present to data with the computer printer.

We were able to check the errors introduced by manual digitización on the Standard records or in automatically digitized data of the tapes for the HGLP case.

COMPUTATION OF THE AMPLITUDE SPECTRA

A computer program for the calculation of the Fourier transform was adapted to obtain the data from the tapes in the case of the HGLP. Again, the program of plotting the spectrum was used but for a better presentation we redraw the points joined by straight lines. Examples of such spectra are shown in figures 1 and 2 for the Standard records and figures 3, 4 and 5 for the HGLP system.

After the Fourier amplitude spectrum of the seismogram has been computedt must be corrected for the instrumental effects if the stations have instruments of different characteristics. To determine the attenuation coefficient K it is not necessary to correct for instrumental effects if the seismographs at all stations have the same characteristics, or if the method of observaing several succesive passages of the same wave at a single station is used. We will discuss later on about this method which clearly point to the HGLP system as advantageous if an appropiate velocity filter is used. In the present study, instrumental corrections are necessary, because the attenuation is calculated between some reference distance and the observing station and also because all seismographs do not have the same respon-

se characteristics. The latter point is especially important when seismograms of both the WWSS and Canadian networks are used or HGLP from different stations. In the case of WWSS stations, due to the homogeneity of the system and similarity in the shape of the system response curves, the magnifications differ only by a multiplier which does not depend upon the period except for the systems which have a peak magnification at 6000.

For the Canadian network and HGLP systems the corrections are more complicated due to the different response of each instrument. The instrumental response of each station was obtained from the Bulletin published by the Dominion Observatory, Ottawa and the list of amplifications of the HGLP of the Lamont-Doherty Observatory, New York.

ATTENUATION COEFFICIENT AND AMPLITUDE SPECTRA AT A REFERENCE DISTANCE

Following the approach previously described, equation (3) is used to calculates K. A program for least-squares approximation of a function by a polynomial of up to 12 degrees was adopted for a linear fitting, linked with the main program to obtain values of the attenuation coefficient K, the constant C and the standard deviation of K. This fit is obtained for each frequency.

Due to some window effects in the Fourier analysis program and the frequency response of the seismograph, the amplitudes to be fitted at both edges of the selected frequency band are not very reliable. Consecuently poor accuracy may be obtained for K and C at those frequencies.

The values of K, plus or minus one standard deviation, are plotted in figures 6 and 7 to give an idea of the range of probable values of K.

In equation (3), the constant C is the intercept of the straight-line fit to the amplitude spectrum at a frequency W at some reference distance x_1 when a correction is applied for geometric spreading from the source to x_1, but no reduction is made for anelastic attenuation from the source to x_1. A particular value for x_1 does not need to be specified.

A plot of such spectrum provides a possible method to discriminate nuclear explosions from earthquakes as Tsai and Aki (1971 have shown. There is a marked difference between the spectra corresponding to both sources.

ANALYSIS OF RESULTS AND CONCLUSIONS

The proposed method for calculating attenuation coefficient requires a good azimuthal coverage of stations. This condition is satisfyed by the WWSSN but not so well by the HGLP; the problem is further complicated by the failure of operation of some stations at the time of the explosion or by the fact that the calibration curve was not properly known or very poorly defined.

In Figure 8 shows the average value of the attenuation coefficient K for Europe, Canada and the Eastern United States as a function of frequency from the 1966 ,and 1970 explosions and Standard data. A mean value of K of 100×10^{-6} Km^{-1} is found in the frequency range of 0.01 Hz to 0.045 Hz. From here there is an almost linear increase up to 0.10 Hz and about 0.075 - 0.080 Hz. A minimun at 0.05 to 0.06 Hz.has been observed previously by Tryggvason (1965) and Tsai and Aki (1969) and a minimun at about 0.08 Hz is consistent with that also found by Tryggvason (1965). This latter minimun in the data, as observed in the present paper, results specifically from

a good transmission of energy to Canada and the Eastern United States in the frequency range.

It is observed that the polynomial fit is very sensitive to the range of distances between stations, Mezcua (1973). In this sense we observe less scatter in the results when working with stations spread out over large distances rather than the same number of stations being concentrated in a small distance interval. In the case of HGLP data a few stations were used in the fitting for K calculation, giving values with a large standard deviation. For this reason we decide not include them with the set of the data because the lack of homogeneity. An alternative to use the HGLP data for this pourpose is to determine K values by comparing succesive pass throught the same station. With this method, used by many authors with Standard Stations it was necessary to use large magnitude earthquakes and no nuclear ezplosions. Among other studies with this method are Anderson at al (1965), Bäth and López Arroyo (1962), Ben-Menahem (1965), Brune (1962), Oliver (1962), etc. Now, with the HGLP data, however will be possible to get down with the magnitudes to be in the explosion range, enough to investigate.

In relation with the amplitude spectrum at a reference distance, the use of Standard Stations give us a good agreement between the theoretical curve (solid line) and the experimental (dotted line) in Figure 9. This curve corresponds to the 1970 explosion. In this sense the HGLP data shows a clear similarity with the one gathered with the Standard Stations.

- REFERENCES -

ANDERSON, D.L., A. BEN-MENAHEM and C.B. ARCHAMBEAU (1965)
"Attenuation of Seismic Energy in the Upper Mantle"
Journ. Geophys. Res. 70, 1441-1448

BÅTH, M. and LÓPEZ ARROYO, A. (1962)
"Attenuation and Dispersion of G wave"
Journ. Geophys. Res. 67, 1933-1942.

BEN-MENAHEM, A. (1965)
"Observed Attenuation and Q values of Seismic Surface Waves in the Upper Mantle"
Journ. Gephys. Res. 70, 4641-4651.

BRUNE, J.N. (1962)
"Attenuation of dispersed wave Trains"
Bull. Seism. Soc. Amer. 52, 109-112

EWING, M., W.S. JARDETZKY and F. PRESS (1957)
"Elastic waves in Layered Media"
McGraw-Hill Book Company, Inc., 127-147

MEZCUA, J. (1973)
"Anelasticidad de la Tierra mediante Ondas Superficiales"
Doctoral Thesis, Universidad Complutense, Madrid

OLIVER, J. (1962)
"A Summary of Observed Seismic Surface Wave Dispersion"
Bull. Seism. Soc. Amer. 52, 81-86

TRYGGVASON, E. (1965)
"Dissipation of Rayleigh Wave Energy"
Jour. Geophys. Res. 70, 1449-1455

TSAI, Y. and K. AKI (1969)
"Simultaneous determination of the Seismic Moment and Attenuation of Seismic Surface Waves"
Bull. Seism. Soc. Amer., 59, No. 1, 275-287

TSAI, Y. and AKI, K. (1971)
"Amplitude Spectra of Surface Waves from Small Earthquakes and Underground Nuclear Explosions"
Journ. Geophys. Res. 76, 3940-3952

TABLE 1

LIST OF EXPLOSIONS USED WITH HGLP STATIONS

DATE	ORIGIN TIME	COORDINATES	MAGNITUDE (MS)
27 September 1971	05 59 55.2	73.4°N 55.1°E	6.4
28 August 1972	05 59 56.5	73.3°N 55.1°E	6.3
21 September 1972	15 30 00.2	37.08°N 116.037°W	5.7
12 September 1973	06 59 54.3	73.3°N 55.2°E	6.8
27 October 1973	06 59 57.4	70.8°N 54.2°E	6.9

LIST OF EXPLOSIONS USED WITH STANDARD STATIONS

DATE	ORIGIN TIME	COORDINATES	MAGNITUDE (MS)
27 October 1966	05 57 57.7	73.4°N 54.9°E	6.3
14 October 1970	05 59 57.1	73.3°N 55.1°E	6.7

- LIST OF FIGURES -

- - - - - - - - -

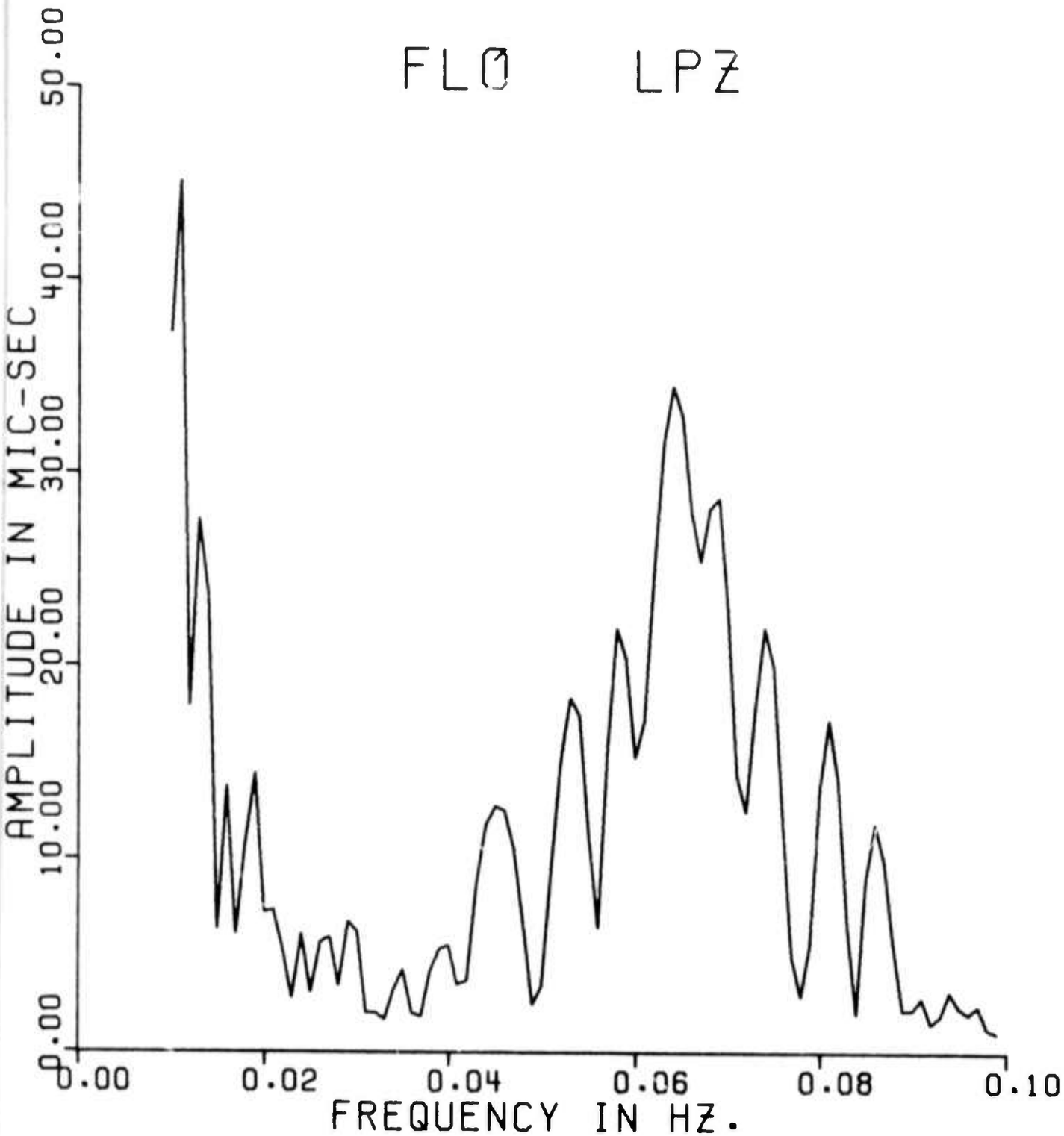
FL0 LPZ
AMPLITUDE IN MIC-SEC
0.00
10.00
20.00
30.00
40.00
50.00
0.00
0.02
0.04
0.06
0.08
0.10
FREQUENCY IN HZ.

FIGURE 1

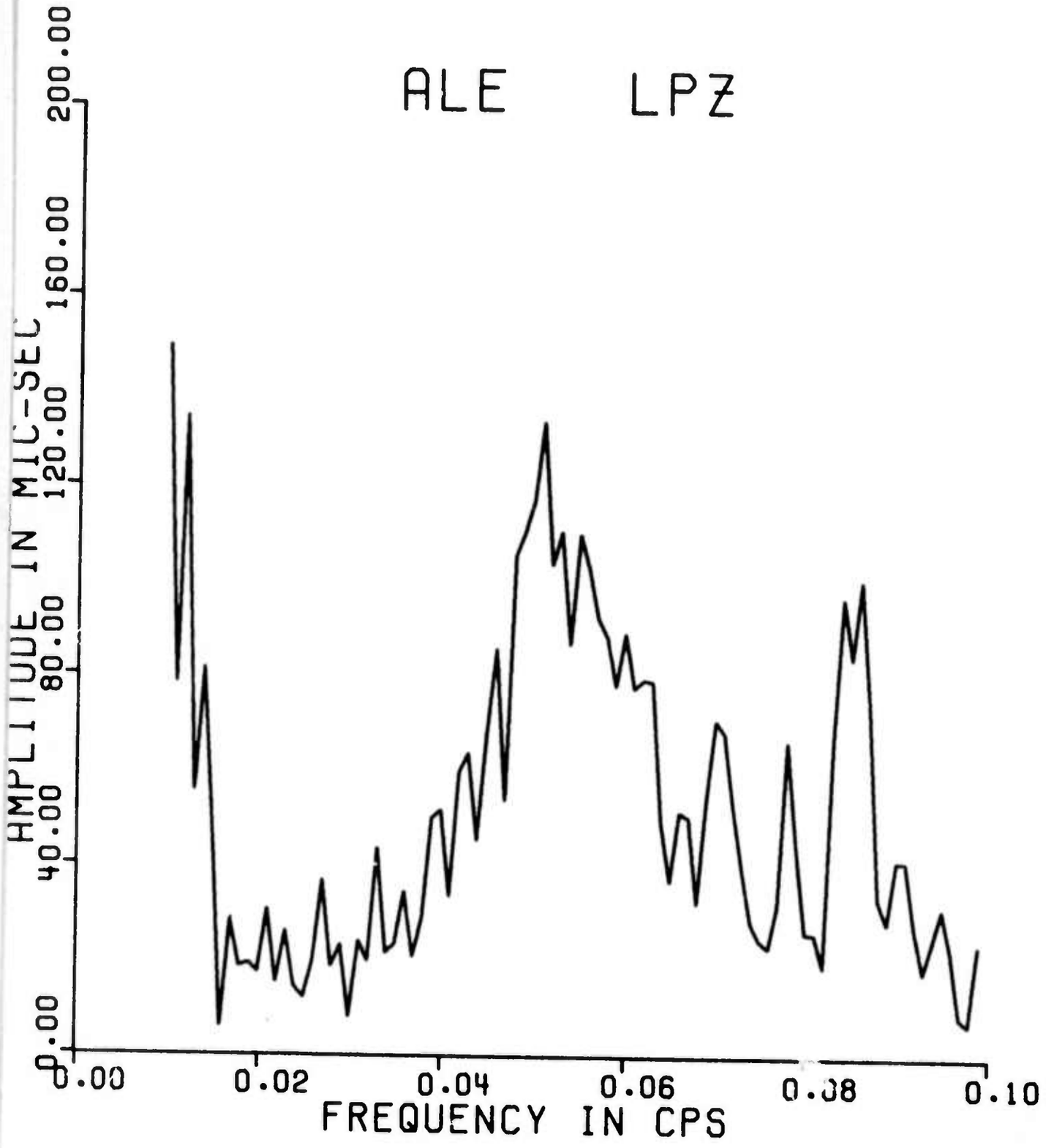
ALE LPZ
AMPLITUDE IN MIC-SEC
0.00
40.00
80.00
120.00
160.00
200.00
0.00
0.02
0.04
0.06
0.08
0.10
FREQUENCY IN CPS

FIGURE 2

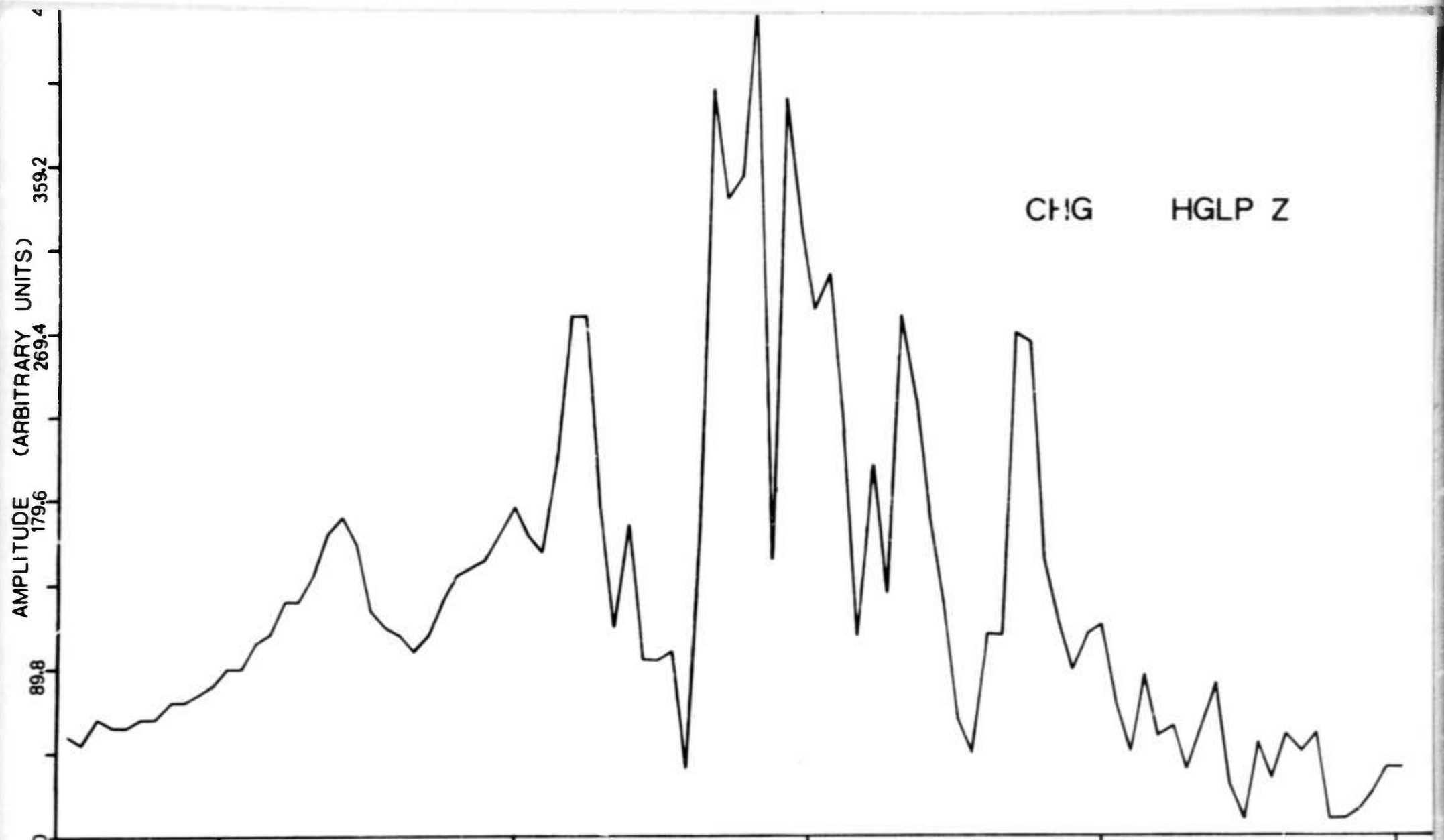
CHIG HGLP Z
AMPLITUDE (ARBITRARY UNITS)
0
89.8
179.6
269.4
359.2
0.02
0.04
0.06
0.08
0.10
FREQUENCY (HZ)

FIGURE 3

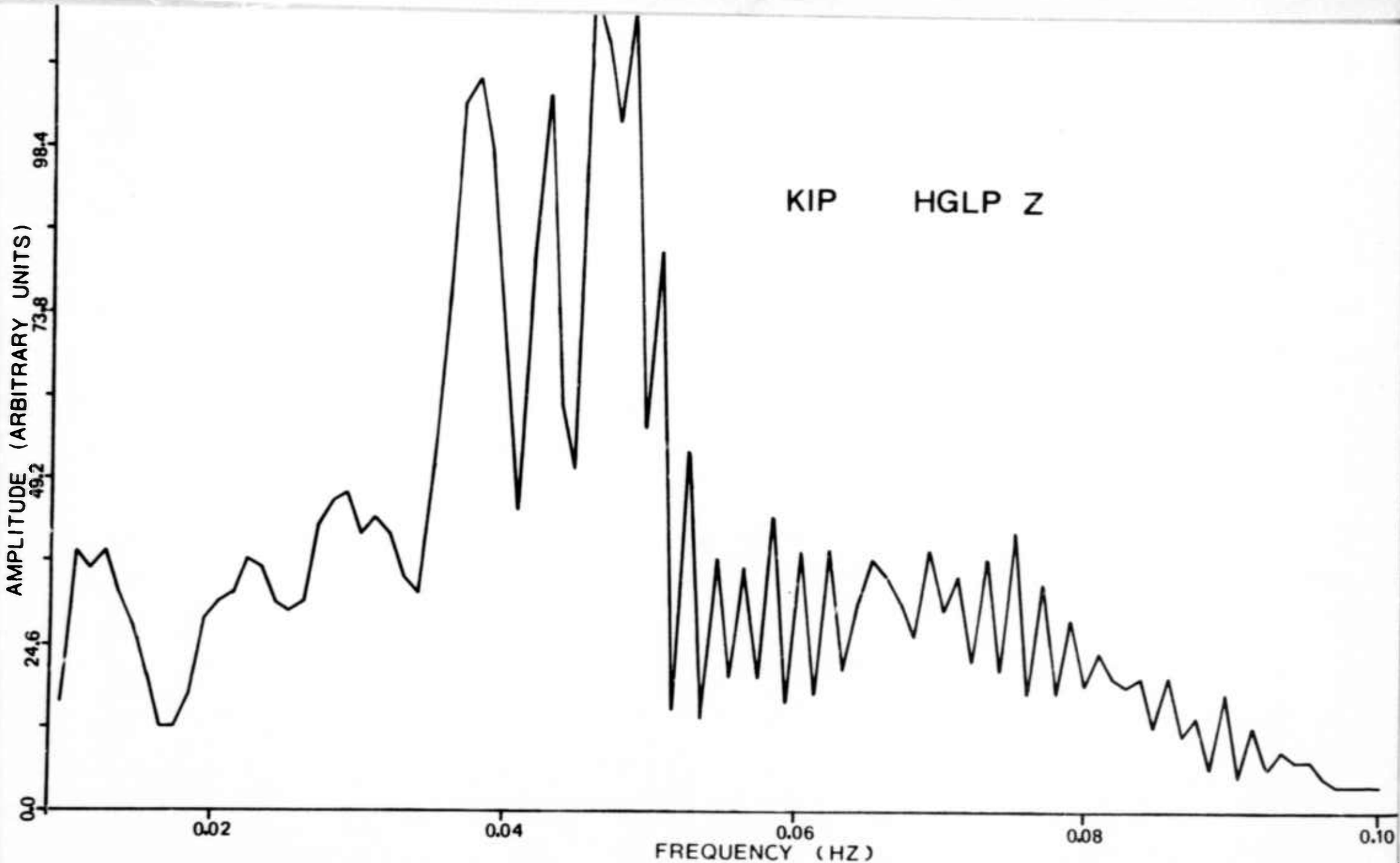
KIP HGLP Z
AMPLITUDE (ARBITRARY UNITS)
0.0
24.6
49.2
73.8
98.4
0.02
0.04
0.06
0.08
0.10
FREQUENCY (HZ)

FIGURE 4

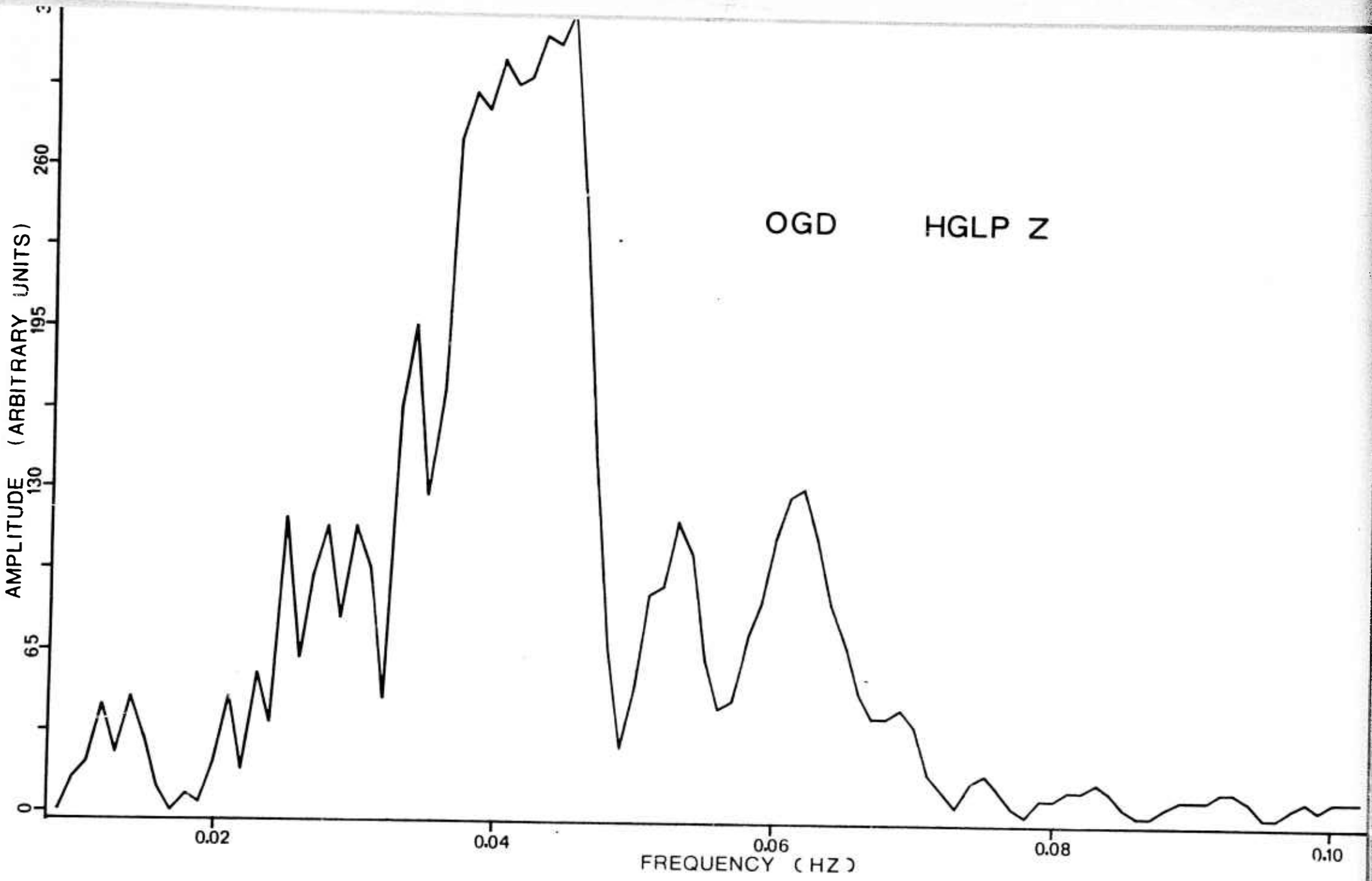
OGD HGLP Z
AMPLITUDE (ARBITRARY UNITS)
0
65
130
195
260
0.02
0.04
0.06
0.08
0.10
FREQUENCY (HZ)

FIGURE 5

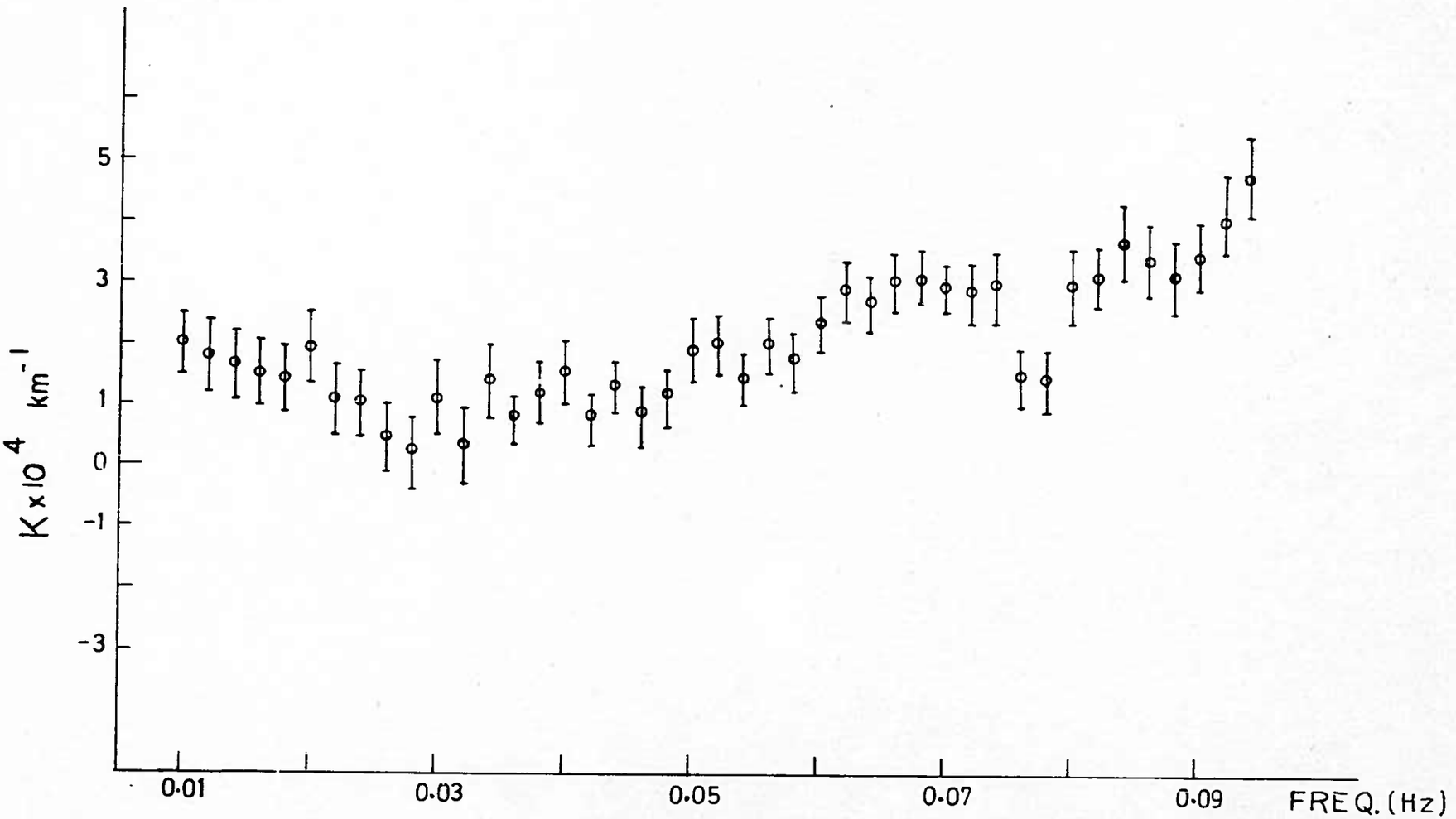

FIGURE 6

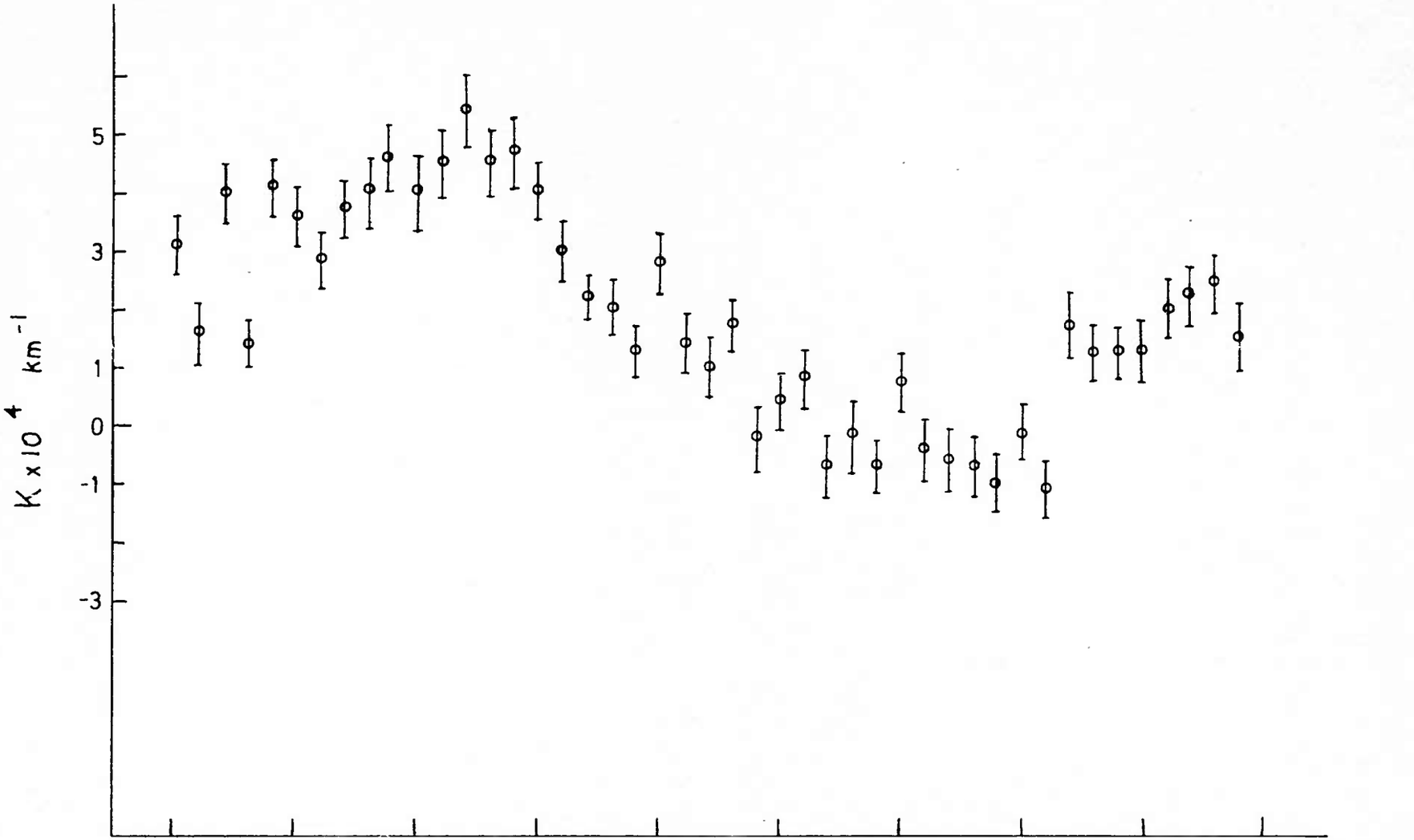

FIGURE 7

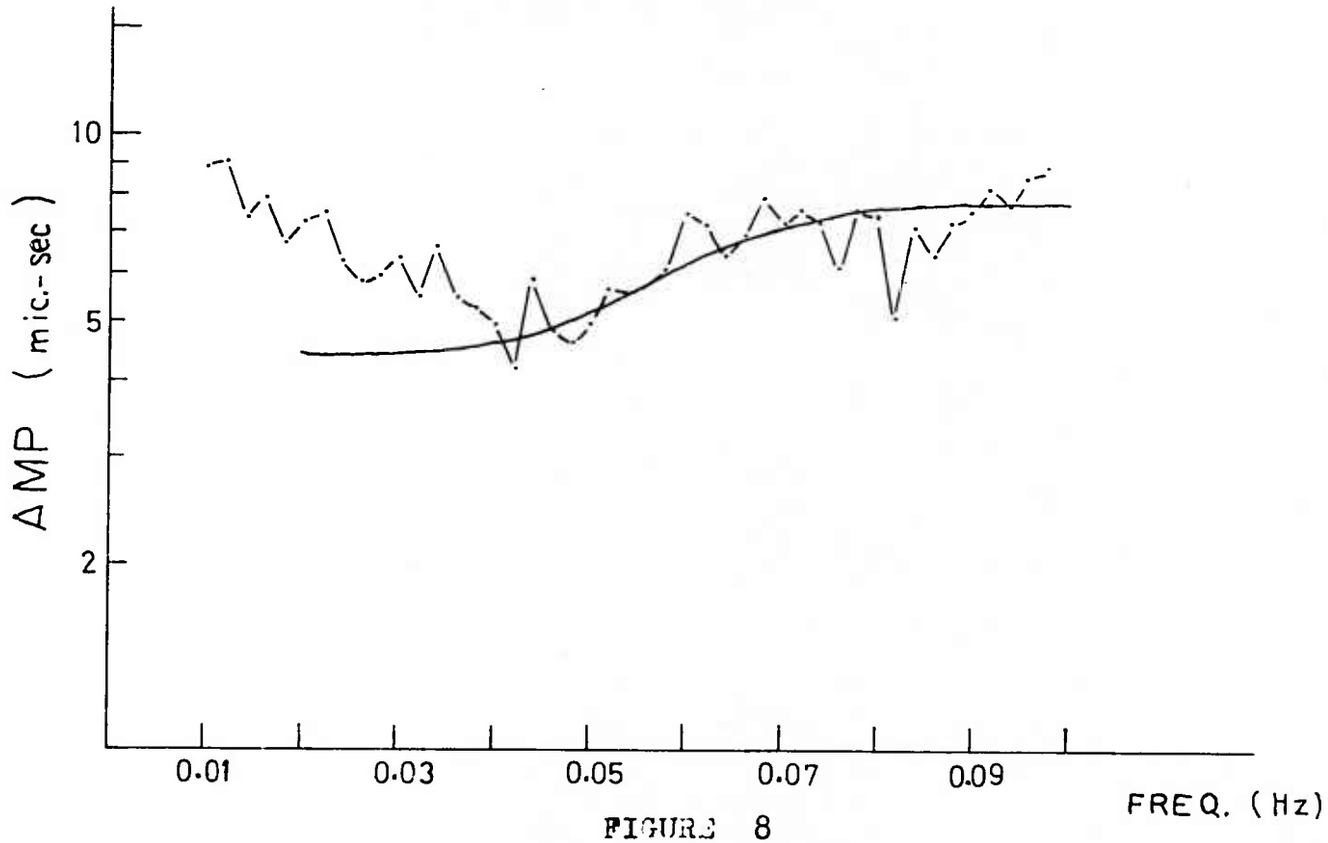

FIGURE 8

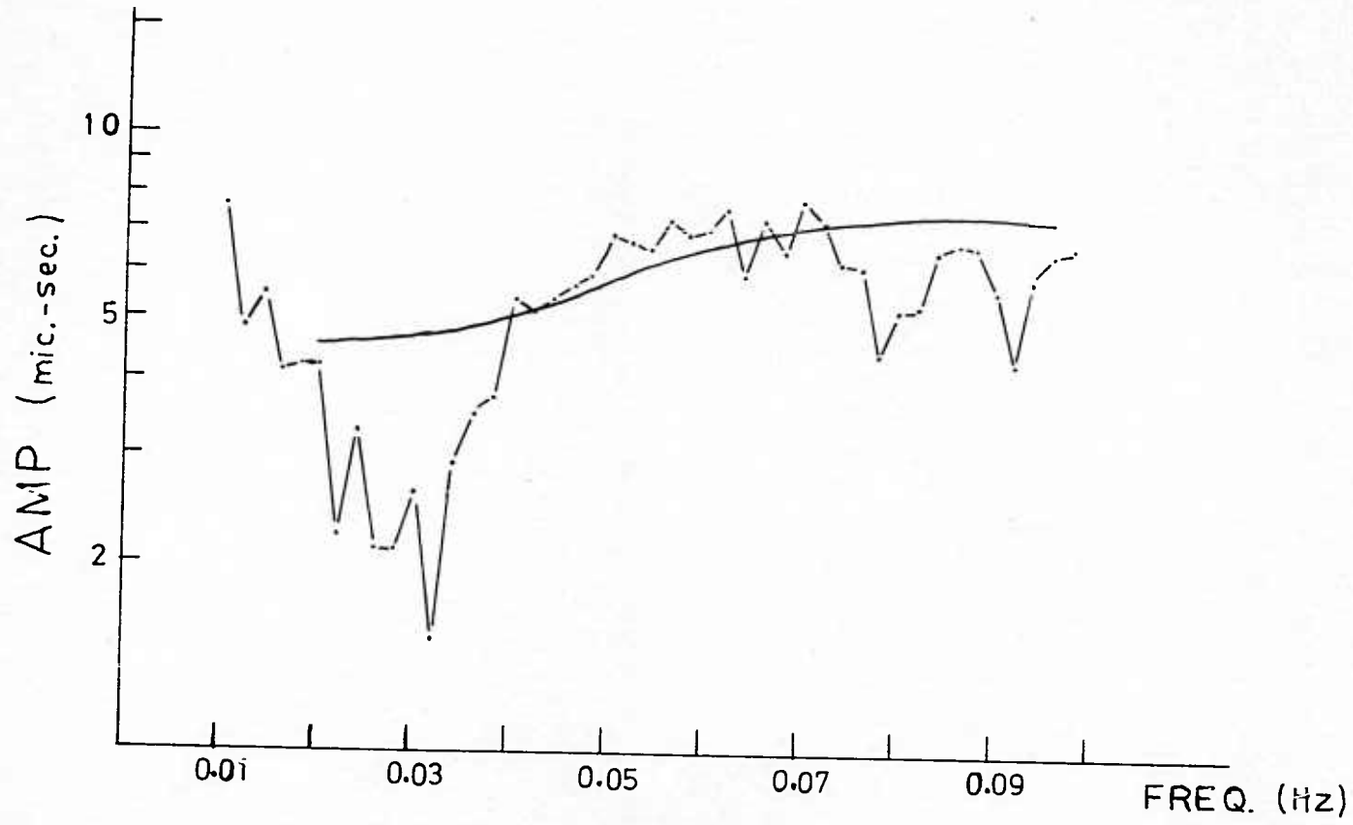

FIGURE 9

DEEP STRUCTURE OF THE MEDITERRANEAN SEA BY SURFACE WAVES DISPERSION

Gonzalo Payo, Eliseo Ruiz de la Parte and Jesús Sierra. Observatorio de Toledo.

INTRODUCTION

Though in the last years several papers have been written about the nature of the crust and upper mantle of the Mediterranean Sea, the structure of this area is still not well known in detail. Figure 1 summarizes most of the works concerning the upper structure of the Mediterranean Sea, showing the models proposed, by different authors (see References), for the Mediterranean crust, according their results obtained by surface wave studies or explosion seismology. Lately some papers have been also made, summarizing the knowledge about the whole structure of the region and its geologic evolution (Ryan et al. 1969; Finetti& Morelli 1973, Payo 1975). The mediterranean area appears very complicated and it cannot be considered as a homogeneous structure since the inner seas (Balearic, Alboran, Tirrene, Jonic, Adriatic, etc) have had different origins and, presently, their crustal structure shows also notable differences. In some of our previous papers (Payo 1967, 1969) we found a great structural difference between the West Mediterranean, with a crust almost oceanic, and the East Mediterranean which appears with a crust of a more continental type, having a thick sedimentary layer.

One of the parts less known of the Mediterranean structure and possibly the most homogeneous one, is that corresponding to the upper mantle. That is the reason why the present work try to study this deep structure along some mediterranean paths, by using the surface wave dispersion methods. The Rayleigh wave phase velocity will be studied, considering the propagation of the surface waves between each pair of long period stations located in the Mediterranean borders.

In the first part of the work, we have used the two high gain long period stations (HGLP) existing in the region, Toledo (Spain) and Eilat (Israel). The characteristics of these stations, of a very long period and high gain (Savino, J.M. et al. 1972) offer important advantages for this kind of studies. First of all their particular location permits to study a long profile (TLO-EIL) that crosses longitudinally the whole Mediterranean area (see Figure 1). The long period of this system (Tg=100 sec., Tp=30 sec.) makes possible to record Rayleigh waves of a long period, even from earthquakes of moderate magnitude. Finally, the agreement of the path TLO-EIL with the ones between the WWSS standard stations TOL-HLW and TOL-JER, permits to

compare the information given by both system of equipments (HGLP and WWSS) and discuss the advantages relative to each of them, for the study of the crust-mantle structure.

A second part of this work was scheduled to study, the other mediterranean paths that can be formed by using pairs of standard stations located on the borders of the Sea (as Toledo, Malaga, Aquila, Jerusalem, Helwan and Athens).

In this report, however, only the part of the results concerning to the HGLP stations is shown, because the data of these station are the only ones we have had time enough to process. Nevertheless, the reproduction and digitation of the standard seismogramshas been already made for all the pairs of standard stations. This report, therefore, only shows some provisional result of the whole work.

We must say that the rhythm of the work has been interrupted several times by different causes. For instance, the difficulty of getting acceptable data from the digitation of the magnetic tapes, filed in the Lamont-Doherty Observatory, where we went to pick up them. This work was scheduled from the beginning, by assuming that the magnetic tapes of the HGLP system could be readily used to get the digitation of the wave trains. The impossibity of using the tape data has led to the necessity of digitizing afterwards the seismograms directly from enlarged microfilm copies, with the corresponding delay in the work to doing that. Other additional trouble for this cause, has arised with the difficulty in digitizing large amplitude seismograms, which had been avoided if the digitation had been obtained from the magnetic tapes. The existence of these large amplitudes has forced, sometimes, to reject the fundamental mode in several cases. Another delay in the work was produced by the change of computer in the Center were the programs were being processed, since the IBM 7090 was substituted by an IBM 360/65. Therefore, when the programs had been prepared for the first computer we had to repeat all the process of adaptation of the programs to the new computer. That substitution produced also a period of more than three months of inactivity in the Processing Center.

THE DATA

All the earthquakes, whose epicenters were lined up with the stations TLO and EIL have been examined from 1971 (date of installation of the HGLP system) up to the present. Only six earthquakes for the profile Toledo-Eilat and three for the reverse profile were finally accepted. The optimum records for this kind of studies, where the Rayleigh fundamental mode is used, correspond to earthquakes which epicentral distances are about 5 to 10 thousand km

from the closest station. In this sense the seismic zones lined up with Toledo and Eilat (South America and the Indian Ocean) are not seismically very active (specially the last one), which makes difficult to find a large number of appropriate seismograms.

In most cases the Rayleigh fundamental mode has been used, being the two stations considered at some 15 wave lengths of distance, relative to the largest period visible on the seismogram. This distance is somewhat large with relation to the wave-length, since the optimun values correspond to distances about 3 to 6 wave-lengths. However, the filtering techniques and the methods of cross-multiplication for determining the phase velocity, may lead to good results. Also we have used waves of great periods, as the surface waves R_2 and R_3 (Rayleigh wave giving turns around the Earth), to compensate the large distance between Toledo and Eilat.

Most of the digitation of the seismograms has been made with an automatic digitizer, that takes the readings from the enlarged microfilm copies, when we follow the signal by means of an optic pointer. The readings have been made every second for the fundamental mode and every two seconds for R_2 and R_3 waves. The pairs of seismograms corresponding to the standard stations (13 cases in total) have been digitized in the same manner.

From the nine earthquakes, above mentioned, corresponding to the HGLP stations (TLO-EIL), four of them shown R_2 and R_3 wave, besides the fundamental mode. However, some of these cases were unfortunately rejected, due to the difficulty in digitizing the large amplitudes of some of the seismograms. Therefore, the subsequent analysis has been only applied to five cases of fundamental mode, five of R_2 waves and one case of R_3 waves.

A program for multiple filtering (Dziewonski et al. 1969) was applied to all these cases. The program reduces the digitized values to the average of them, removes the linear trend, computes the Fourier transform (algorithem of Cooly & Tukey) and applies, along the seismogram, a gaussian filter truncated at 30 db and with a bandwidth proportional to the frequency. Finally, the program gives the energy-density diagrams as a function of the group velocity and the logarithm of the period. Figures 3a a 3b show an example of the diagrams obtained, corresponding to the same earthquake recorded at the two stations.

Regarding the results of all these group velocity diagrams, some of the cases with little energy or with the contour lines not well defined have been rejected. The rest of the cases accepted appear in the next table.

TABLE I

DATE	ORIGIN TIME h m s	φ λ	FIRST STATION	SECONO STATION	TYPE OF WAVE	REGION
7-Sep-72	02-54-58	2ºOS-68ºOE	EIL	TLO	F. mode	Indian Ocean
16-Sep-72	09-14-34	15º2N-96º2W	TLO	EIL	F. mode	Mexico
23-Dec-72	06-29-42	12º4N-86º1W	TLO	EIL	F. mode	Managua
7-Jun-73	18-34-46	14º2N-91º9W	TLO	EIL	F. mode	Guatemala
16-Sep-72	09-14-34	15º2N-96º2W	EIL	TOL	R_2	Mexico
14-Apr-73	08-34-00	10º7N-84º7W	EIL	TOL	R_2	Costa Rica

The group velocity curves thus obtained for all these cases have been used to get the values of the phase velocity across the path between Eilat and Toledo. For the computation we have used a program of cross-multiplication, FACROS, that from the filtered seismograms at the two stations and by using the group velocity previously obtained, computes the phase velocity for the range of periods 14 to 140 seconds. In general lines, the program operates as follows. First, it computes the arrival time of each period for both seismograms, in order to apply a "window" with a width five times the corresponding period. Next, for each one of the velocities between 3 and 5 km/sec, the program computes the time $\tau_i = (A-B)/c_i$ and it moves one seismogram relative to the other the amount τ_i, making in this position the multiplication of them. The largest of these products is plotted against the period and phase velocity in form of a normalized diagram (see the example of figure 4). The phase velocity curve appears then as the line that joints the maximum values of the diagram. We have designed with thick circles the highest values of each column and with thin circles the other large values close to the maximum .

RESULTS AND DISCUSSION

The phase velocity curves for all the cases finally admitted have been averaged. Figure 5 shows this average (doted line), where the vertical bars

represent the standard deviation for some selected periods. In the figure we have also plotted the curves corresponding to several models to be compared with our results.

As we can see, the curve here obtained shows fairly low velocities for the range of periods between 15 and 35 seconds. This part of the curve is the most reliable one, because the velocities are in good agreement for all the cases. These phase velocities are governed by the shear velocities of the first layers of the Earth, up to some 60 kms of depth, and these low values were already found by the author (Model EME of the Figure) for the eastern Mediterranean Sea. Of course, the present values are somewhat higher than those of model EME, but we have to consider that the path TLO-EIL only has a 60 per cent along this eastern part of the Mediterranean. However the influence of this part, with this thick sedimentary layer that seems to have (Payo 1969), is clearly visible in the dispersion curve, whose values in the short period range are below those corresponding to a typical oceanic model (8099 in the Figure) or a continental model (CANSD).

The rest of the dispersion curve, here obtained, that is the part of the curve between 40 and 110 seconds of period exhibits, however, fairly high values. The phase velocities are comparable to those of the CANSD model, and they are some 0.1 km/sec larger than those of the oceanic model 8099 and about 0.2 km/sec larger than those of the models G1 or G2 given by Berry & Knopoff for the West Mediterranean basin. The interpretation of such high velocities is problematic. It would suppose high shear velocities below the Mohorovicic discontinuity (about 4.7 km/sec) and the absence or little significance of the low velocity channel in the upper mantle. Other posibility is that the channel be located at a depth greater than normal. The flat nature of the curve for periods larger than 80 seconds is in favor of this hypothesis.

These first results will be complemented with future studies about this zone, and they will give new information about the structure of this complex mediterranean region.

Gonzalo Payo Subiza
Eliseo Ruiz de la Parte
Jesús Sierra

Abril, 1975.

Observatorio Geofísico Central
Instituto Geográfico y Catastral
TOLEDO

FIGURE CAPTIONS

Figure 1.- Some of the models obtained for different areas of the Mediterranean sea. LR means Rayleigh waves, LQ Love waves, R refraction profiles, G group velocity methods and F phase velocity methods. The figures without parenthesis are the velocities given directly by the method of investigation used.
Also the path TOL-EIL, studied in this work, appears in this Figure.

Figure 2.- An example of the seismograms used. It corresponds to the earthquake of 7 Sept. 1972, recorded at TLO and EIL with the HGLP seismometers.

Figure 3.- Group velocity curve obtained "multiple filtering" method. The curve appears as the line that follows the maximum energy of the diagram. It corresponds to the earthquake of 16 Sept. 1972, recorded at the TOL (Figure 3a) and EIL (Figure 3b).

Figure 4.- Diagram of the phase velocity curve between TOL and EIL obtained by the cross-multiplication method (see the text). It corresponds to the earthquake of 7 Sept. 1972 in Indian Ocean region.

Figure 5.- Comparison of the phase velocity curves here obtained with those corresponding to some Mediterranean models and with a typical oceanic or continental structure. Models 1 and 2 correspond (Berry & Knopoff, 1967) to the West Mediterranean basin, model 3 (Payo, 1969) to the Eastern part of the Sea, model 4 is an Atlantic model (Dorman et al. 1960) and model 5 a typical continental model, (Brune and Dorman 1963).

REFERENCES

BERRY, M.J., KNOPOFF, L. (1967). "Structure of the Upper Mantle under the western Mediterranean Basin". J. Geophys. Res., Vol. 72, 3613-3627.

BRUNE, J. DORMAN, J. (1963). "Seismic Waves and Earth Structure in the Canadian Shield". Bull. Seismic. Soc. of Am. Vol. 53., núm. 1, 167-210.

DZIEWONSKI, A., BLOCH, S., LANDISMAN, M., (1969). "A technique for the Analysis of transient Seismic signals". Bull. Seism. Society of Am., vol. 59, núm. 1.

EWING, M., BRUNE, J., KUO, J. (1962). "Surface-Wave Studies of the Pacific Crust and Mantle". Crust of the Pacific Basin, Geophysical Monograph, núm. 6.

FAHLQUIST, D.A., (1963). "Seismic refraction studies in the western Mediterranean" Abstract of the Ph. D. Thesis, M.I.T. Cambrige (Mass.)

FAHLQUIST, D.A. Hersey, J.B. (1969). "Seismic refraction measurements in the western Mediterranean Sea". Bull. Inst. Oceanographic (Mónaco), 67, 1386.

FINETTI, I., MORELLI, C. (1973). "Geophysical Exploration of the Mediterranean Sea". Bull. di Geof. Teor. ed Appli. , Vol. XV, núm. 60.

LORT, J.M., LIMOND, W.Q. GRAY, F. (1974). "Preliminary seismic studies in the Eastern Mediterranean". Earth and Planetary Science Letters, 21, 355-366.

PAPAZACHOS, B.C. (1968). "Phase velocities of Rayleigh waves in Southeastern Europe and Eastern Mediterranean Sea. Manuscrito.

PAYO, G. (1967). "Crustal structure of the Mediterranean Sea by surface waves. Part I: Group velocity". Bull. Seismic. Soc. Am. vol. 57, núm. 2, 151-172.

PAYO, G. (1969). "Crustal structure of the Mediterranean Sea. Part II: Phase velocity and Travel Times". Bull. Seism.Soc. of Am. Vol. 59, núm. 1, 23-42.

PAYO, G. (1975). "Estructura, Sismicidad y Téctónica del Mar Mediterraneo". Publicación del Instituto Geográfico y Catastral. Madrid.

RYAN, W.B.F., STANLEY, D.J.; HERSEY, J.B.; FAHLQUIST, D.A. & ALLAN, T.D., (1969). "The Tectonics and Geology of the Mediterranean Sea". Lamont-Doherty Geological Observatory Contribution, núm. 1.469.

SAVINO, J.M., MURPHY, A.J., RYNN, J.M., TATHAM, R., SYKES, L.R., CHOY, G.L., MCCAMY, K. (1972). "Results from the high-gain long-period (HGLP) seismograph experiment. R.A.S. Geoph. Jour. V. 31, Nos. 1-3.

WEIGEL, W. HINZ, K. (1971). "Preliminary result of seismic measurements in the Jonian Sea and on the Malta Shell. XII Assemblée Générale de la Comission Seismologique Européenne. (Obs. Roy. Belg.).

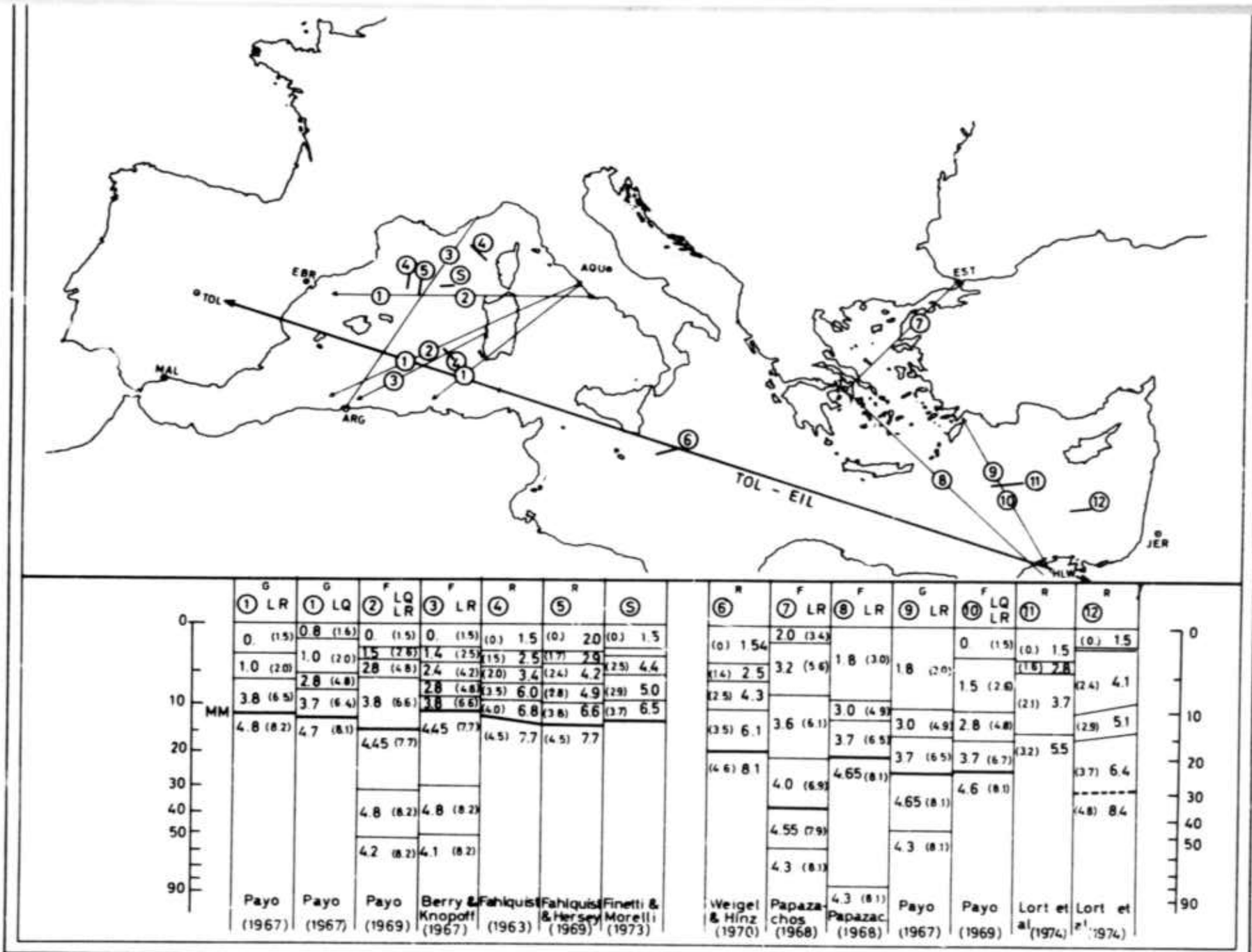
EBR
TOL
MAL
ARG
AQUe
EST
JER
HLW
TOL - EIL
MM
0
10
20
30
40
50
90
① G LR
① G LQ
② F LQ LR
③ F LR
④ R
⑤ R
⑤
⑥ R
⑦ F LR
⑧ F LR
⑨ G LR
⑩ F LQ LR
⑪ R
⑫ R
Payo (1967)
Payo (1967)
Payo (1969)
Berry & Knopoff (1967)
Fahlquist (1963)
Fahlquist & Hersey (1969)
Finetti & Morelli (1973)
Weigel & Hinz (1970)
Papazachos (1968)
Papazac. (1968)
Payo (1967)
Payo (1969)
Lort et al (1974)
Lort et al (1974)

Fig. 1

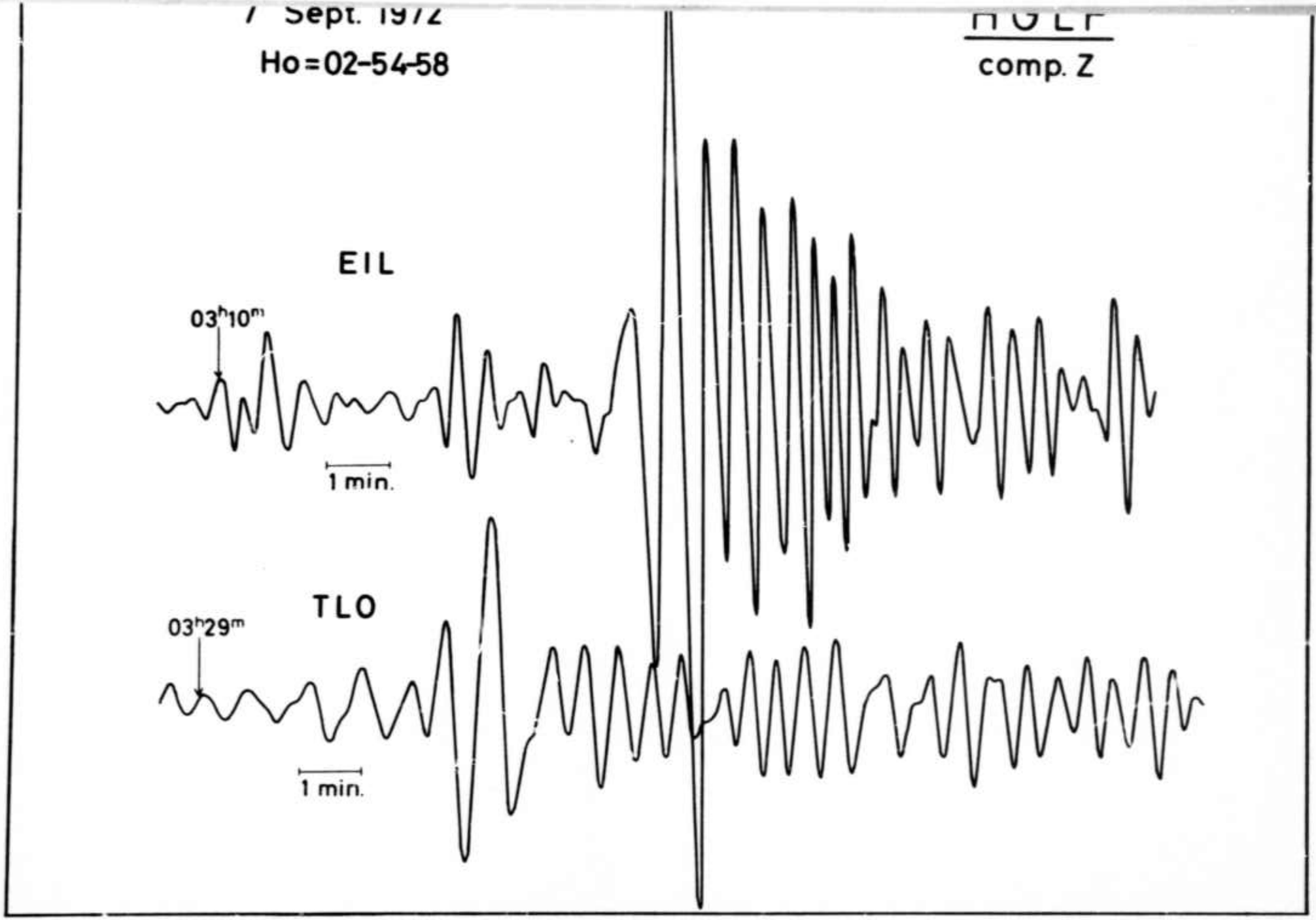
7 Sept. 1972
Ho=02-54-58
HGLP
comp. Z
EIL
03h10m
1 min.
TLO
03h29m
1 min.

Fig. 2

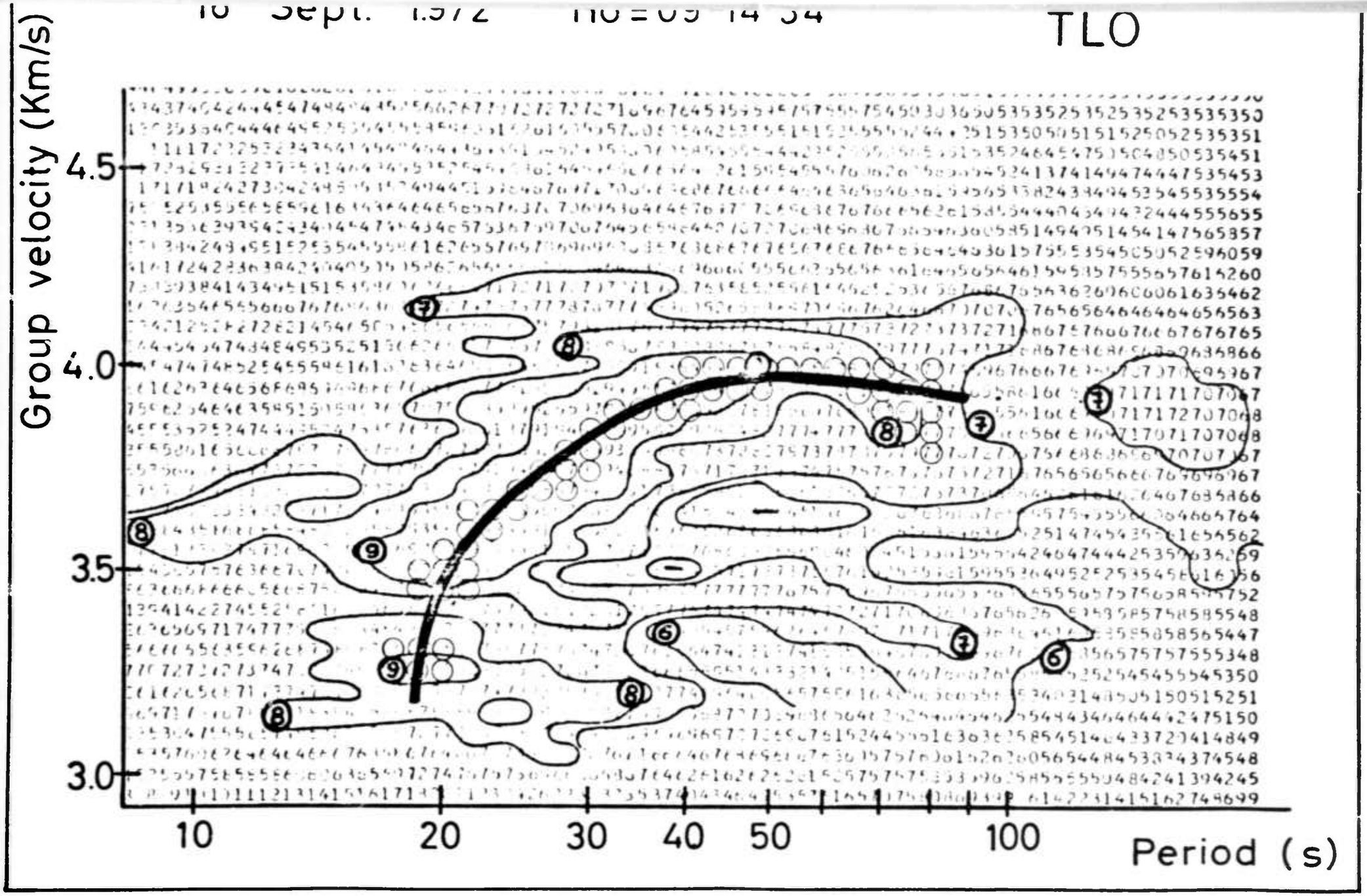

Fig. 3a

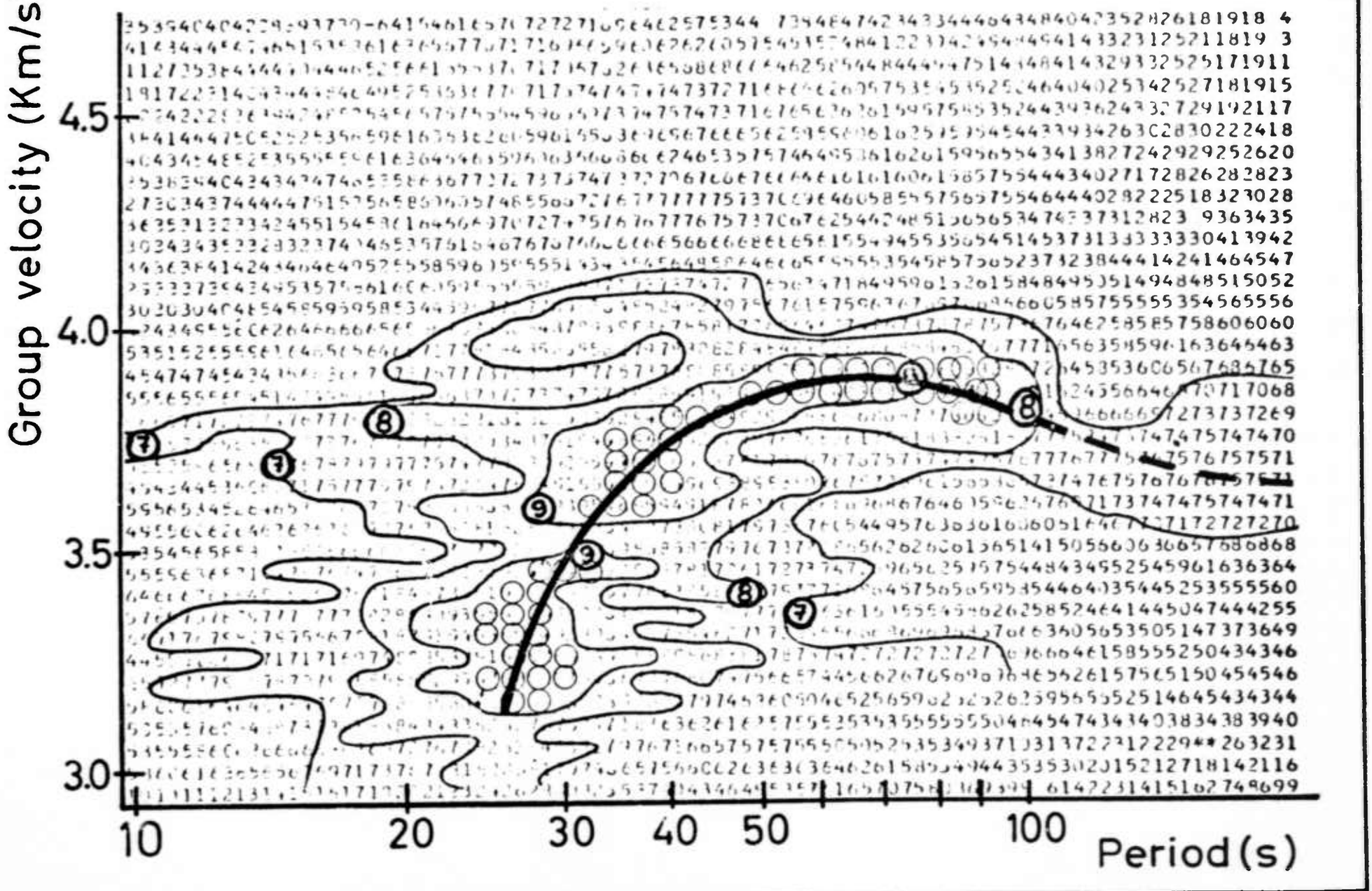

Fig. 3b

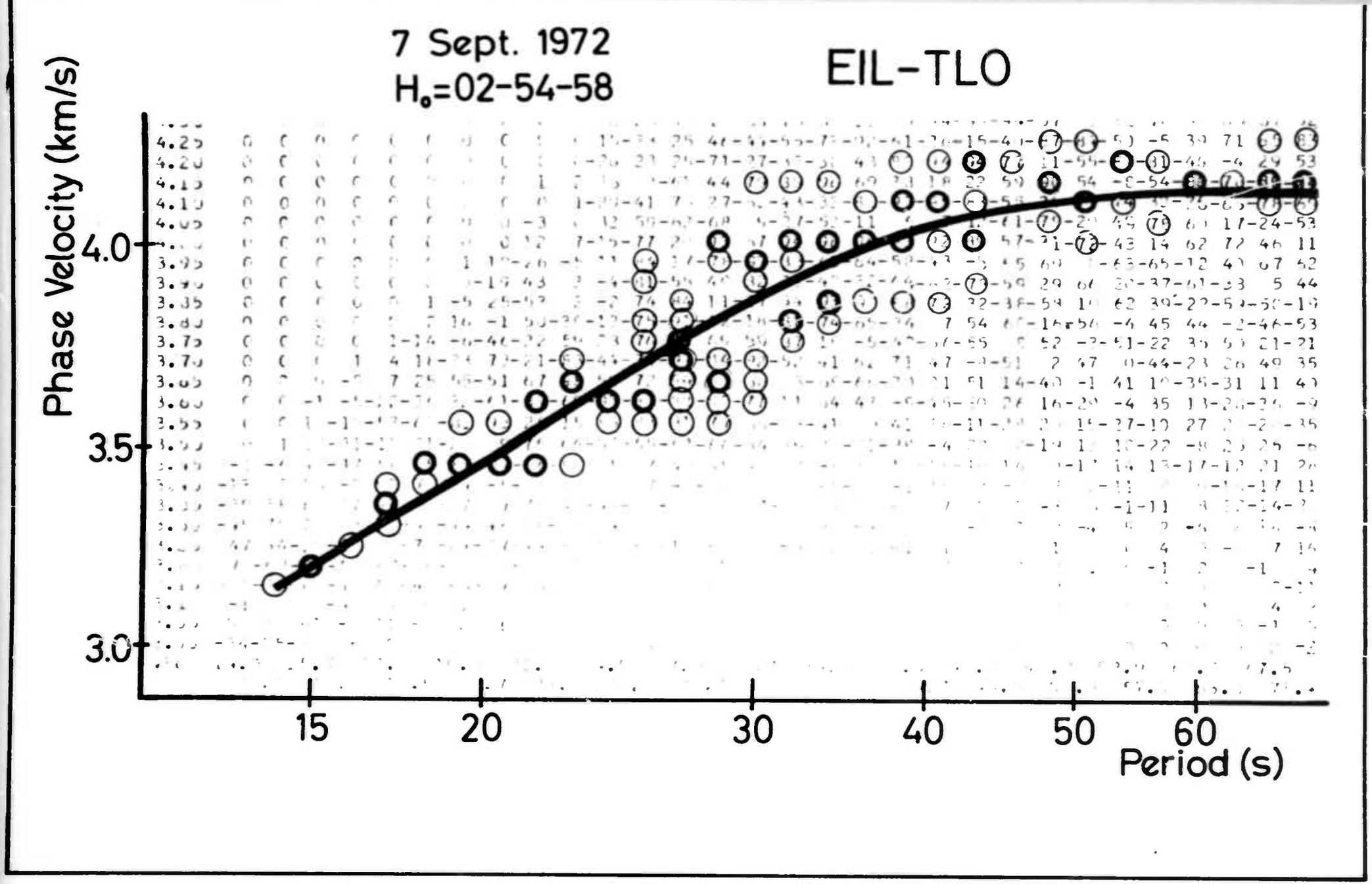
7 Sept. 1972
H₀=02-54-58
EIL-TLO
Phase Velocity (km/s)
4.0
3.5
3.0
15
20
30
40
50
60
Period (s)

Fig. 4

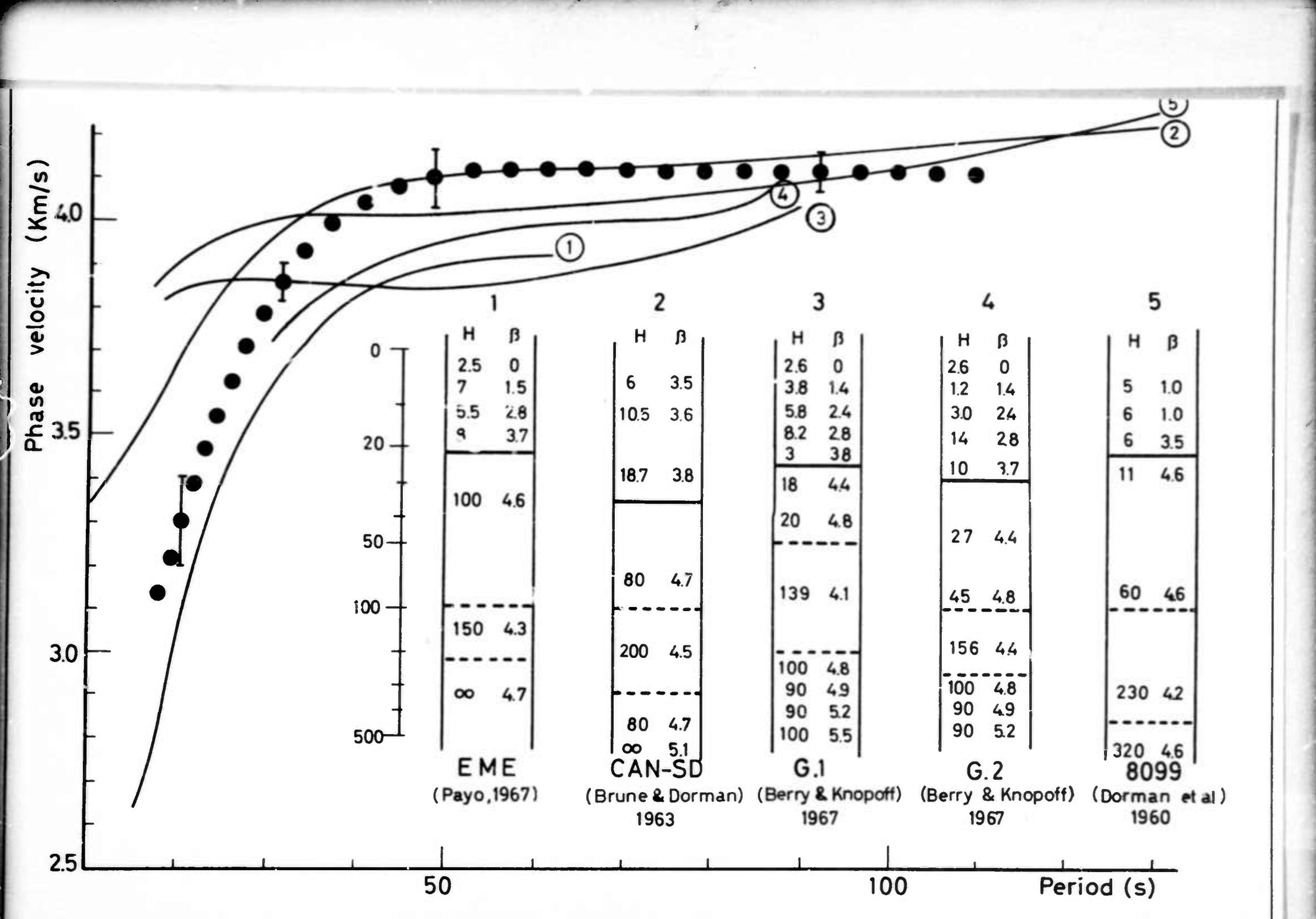
Phase velocity (Km/s)
4.0
3.5
3.0
2.5
50
100
Period (s)
1
2
3
4
5
0
20
50
100
500
H β
2.5 0
7 1.5
5.5 2.8
9 3.7
100 4.6
150 4.3
∞ 4.7
EME
(Payo, 1967)
H β
6 3.5
10.5 3.6
18.7 3.8
80 4.7
200 4.5
80 4.7
∞ 5.1
CAN-SD
(Brune & Dorman)
1963
H β
2.6 0
3.8 1.4
5.8 2.4
8.2 2.8
3 3.8
18 4.4
20 4.8
139 4.1
100 4.8
90 4.9
90 5.2
100 5.5
G.1
(Berry & Knopoff)
1967
H β
2.6 0
1.2 1.4
3.0 2.4
14 2.8
10 3.7
27 4.4
45 4.8
156 4.4
100 4.8
90 4.9
90 5.2
G.2
(Berry & Knopoff)
1967
H β
5 1.0
6 1.0
6 3.5
11 4.6
60 4.6
230 4.2
320 4.6
8099
(Dorman et al)
1960

Fig. 5